Joint Centre for Mesoscale Meteorology, Reading, UK

Odservations of the mesoscale sub-structure in the cold air of a developing frontal cyclone

K. A. Browning
S. A. Clough
C. S. A. Davitt
N. M. Roberts
T. D. Hewson

Internal Report No. 33

May 1994

Met Office Joint Centre for Mesoscale Meteorology Department of Meteorology
University of Reading PO Box 243 Reading RG6 6BB United Kingdom
Tel: +44 (0)118 931 8425 Fax: +44 (0)118 931 8791
www.metoffice.com

Version : May 94

Observations of the mesoscale sub-structure in the cold air of a developing frontal cyclone

K A Browning, S A Clough, C S A Davitt, N M Roberts and T D Hewson

University of Reading, UK

Summary

Observations from 58 dropsondes released in a mesoscale array during the FRONTS-92 experiment are interpreted in the context of satellite imagery to derive the mesoscale structure and evolution of a frontal cyclone developing over the north Atlantic. A conceptual model involving the intertwining of 'dry intrusion' and 'cloud head' flows is corroborated and is used to provide the framework for interpreting the detailed mesoscale behaviour. In the cold air, two distinct dry intrusions were found to be responsible for two cold fronts, trailing southwestwards from the tip of the cloud head. Both were surface features at the beginning of our study but the leading one evolved into an upper front with mid-level convection as the dry intrusion responsible for it overran the warm sector. The dry intrusions contained poorly resolved pockets of

---

*Corresponding author: Joint Centre for Mesoscale Meteorology, Harry Pitt Building, University of Reading, Whiteknights Road, PO Box 240, Reading, RG6 2FN, UK. (The Joint Centre for Mesoscale Meteorology is supported by the Meteorological Office and the Department of Meteorology, University of Reading.

low (and in some places negative) potential vorticity which, upon encountering a critical level of zero system-relative velocity, led to the development of multiple dry/moist laminae near the top of the boundary layer. The vertical wavelength of the laminae was about 1 km and they extended over 200 km in the front-normal direction, with a slope of typically 1 in 60. Although most parts of the laminae were subsaturated, their circulations combined with the double structure of the dry intrusions to produce multiple shallow cloud lines within the boundary layer.

1. Introduction

A conceptual model of a developing frontal cyclone or frontal wave has been developed by Browning and Roberts (1994) to integrate a number of well known features such as warm and cold conveyor belts, split fronts and frontal fracture, and the dry intrusion and cloud head. In its simplest idealization, omitting the part of the warm conveyor belt flow that ascends above the warm front, their model reduces to that shown in Fig 1 in which the cyclone develops in the region where the two hammer-head shaped flows interlock. One of these flows consists mainly of moist ascending air which leads to the characteristic cloud head with well defined leading edge as seen in satellite imagery. The other flow consists of dry air that has descended from the upper troposphere and/or lower stratosphere, with the leading edge of this dry intrusion corresponding to the cold front. The two flows mirror each other in developing rather well defined convex leading edges.

The overall structure implied by Fig 1 sets the scene within which a number of mesoscale features occur which have an important effect on the weather. At first sight the mesoscale structure may appear to be complex. However, satellite and radar imagery, interpreted in a light of a conceptual model and NWP model output, can often provide a good indication of the processes at work and of the associated weather. The purpose of this paper is to present a case study that accounts for the mesoscale structure particularly in the region where the two major flows in Fig 1 interlock. Whereas the study by Browning and Roberts relied heavily on NWP model output, the present study will rest almost entirely on observational data. The observations are shown not only to support the earlier conceptual model but also to add considerable detail on the mesoscale.

The unique contribution to this paper comes from a set of 58 dropsondes released from a research aircraft in the vicinity of a developing cyclone over the north Atlantic during the FRONTS 92 project. These are analyzed together with the imagery to reveal the fine structures within the dry intrusion, or rather two dry intrusions in close succession. The analyses also reveal in detail how the dry intrusions interacted not only with the moist air ahead of them but also with the moist air that was recirculating cyclonically to the north of the cyclone centre, within the (southwestern) tip of the cloud head. Relationships are established that are believed to have some generality for developing frontal cyclones. The cyclone in the present study was deepening fairly rapidly but it was not an unusually intense development. For 18 hours the cyclone retained an almost constant central pressure while the cloud head began to form (Fig 2). Then, between 12 UT on 27 April and 00 UT on 28 April 1992, the cyclone deepened by 12 mb and, by the end of this period, the cloud head had acquired a characteristically well-defined convex outer edge. The dropsondes were released between 12 and 21 UT on 27 April; shortly afterwards the system was observed by land-based radiosondes and radars.

2. The dropsonde data

The flight track of the Meteorological Research Flight C-130 aircraft during Intensive Observational Period 3 of FRONTS 92 is shown in Fig 3, with positions and times of soundings marked. The dropsondes in this flight were similar to those used in the FRONTS 87 project (Thorpe and Clough 1991), though with an improved pressure sensor. The main difference was that sondes had to be released from a lower altitude (6.1 km) because of conflicting air traffic. Full details of the FRONTS 92 experiment are presented in Hewson (1994).

Data analyses were prepared for the dropsonde observing area by assigning a standard analysis time of 18 UT on 27 April, the main synoptic hour nearest to the mid-time of the observations. This allowed a corresponding surface pressure analysis to be derived from available synoptic observations. The system-relative locations of the dropsondes at 18 UT, as shown in Fig 3, were calculated by displacing actual sounding positions with a system velocity of 19 ms^{-1} along a bearing of 73 deg. This velocity was deduced from forecast positions of the low pressure centre but is 3 ms^{-1} less than the mean velocity of the cloud head in the satellite imagery. The uncertainty in the system velocity will affect the details of subsequent analyses but not the main conclusions.

Observations from 14 available ships and 18 land stations were used to carry out a surface pressure analysis using a two-dimensional smoothing spline algorithm (see Thiebaux and Pedder 1987) in order to provide maximum differentiability. Isentropic analyses were also derived from 3-d objective analyses of the dropsoundings. The analyses were carried out using the successive correction algorithms of Pedder (1993), which are computationally more economical for large three-dimensional datasets, and for the specification of filtering properties. For these analyses a linear trend basic state was taken for scalar variables (temperature, wind components and relative humidity) and the method of successive corrections applied to the deviations.

3. Mesoscale structure during rapidly deepening phase

(a) Overview of surface frontal pattern in relation to cloud head.

The surface pressure and frontal analysis for 18 UT, 27 April is shown in Fig 4, with

simplified cloud analysis superimposed. The pressure analysis has been carried out objectively as outlined in Sec 2. The frontal analysis is based upon the detailed evidence presented in later subsections. The cloud analysis is based on the Meteosat imagery. The edge of high cloud associated with the polar front cloud band is identified by a cusped line; so, too, is the northwestern edge of the cloud head, part of which extends out of the diagram to the northeast. We do not discuss the polar front cloud band in this paper, as it was largely above and ahead of the main region of development; rather, we concentrate on the structure and airflow associated with the cloud head and with the two cold fronts that are shown extending southwestward from it. As we shall show, the cold fronts and the cloud head were closely related; the top of the cloud in the cloud head lowered towards its southwestern tip where it merged with the shallow cloud bands associated with the cold fronts.

(b) Visualization of the broad 3-D pattern of airflow.

Key features of the airflow pattern associated with the cyclone are represented in Fig 5 by relative flow within isentropic surfaces as derived from the dropsondes. This diagram is intended only to introduce the reader to the overall flow pattern; more detailed isentropic analyses are given later in connection with Fig 9. The three surfaces shown in Fig 5 are:

(i) $\theta_w = 12$C moist isentropic surface. This shows a saturated flow corresponding to the lower part of the warm conveyor belt (WCB), 200 km wide, ascending from low levels (<1 km) in the warm sector to above 4 km over the warm frontal zone ahead of the cyclone. (The upper part of the WCB, which was responsible for the polar front cloud band (see Fig 4) is not depicted here).

(ii) $\theta_w = 8$C moist isentropic surface. This is one amongst several surfaces in the range $6<\theta_w<10$C which represent the mainly saturated cold conveyor belt

(CCB) flow. Relative to the system, the CCB travelled northwestwards, within and beneath the warm frontal zone. It then fanned out, the northern part turning towards the north and then northeast, and the southern part turning southwestwards within the cloud head just to the north of the cyclone centre. Initially this flow ascended up the isentropic surface but the ascent decreased as it turned southwestward parallel to the slope of the isentropic surface. To the extent that the pattern could be considered to be in a steady state, the flow would be inferred to have then descended down the isentropic surface near the tip of the cloud head. In reality, in a rapidly deepening cyclone this is a poor assumption: the isentropic surfaces were being deformed with time so as to greatly diminish and possibly eliminate the implied descent in this region.

(iii) θ = 25C dry isentropic surface. This shows the northwesterly relative flow characteristic of the deep layer of dry air descending behind the cyclone. It overran part of the cloud head, Cold Front 2 and part of Cold Front 1, and then turned to become an ascending southwesterly flow. Initially the flow was very dry (RH~30%) but the relative humidity increased as it overtook the system. Further evidence of this flow extending ahead of CF1 is shown later in Fig 14.

(c) The two cold fronts,CF1 & CF2

The double cold frontal analysis in Figs 4 and 5 is consistent with dropsondes and satellite imagery. In particular, the double structure is evident in the 950 mb θ_w-pattern shown in Fig 6. It is also evident in the almost north-south vertical section along Run 5 shown later in Sec 5. In the satellite imagery the cold fronts could be seen in both the visible (Fig 7) and infra-red (Fig 8). CF1 is particularly clearly identified in Fig 7 by the

sharply defined dark strip associated with a clearance of the cloud immediately behind the surface front. Fig 8 shows that the band of cloud immediately ahead of CF1 consisted of low clouds with tops ranging from +5C (at the blue-green transition) to -5C (at the medium green-light green transition). For a θ_w of 12C this corresponds to tops between 1.4 and 3.1 km. This cloud band was observed from the C-130 aircraft as a rather smooth-topped line of stratocumulus. Slightly higher (3 km) cloud tops within this line can be seen in Fig 8 to have originated close to the surface position of CF1 and then to have extended forwards at a small angle (about 20 deg) to the front; these features were parallel to the relative airflow at their tops (see θ = 25C flow in Fig 5 overtaking the surface front) and they are analogous to the line elements encountered in narrow cold frontal rainbands. Cold front CF1 extended to the position of the low centre and here the cloud tops rose abruptly to a maximum of 6.5 km (red in Fig 8); this region of deeper convection is discussed in detail in Sec 4(c).

The second cold front, CF2, was rather less distinct to the imagery. In the visible it is seen as a ragged narrow band of cloud. Along part of its length there is another thin line of cloud just ahead of it. To the northeast, these thin lines of cloud merge into the tip of the cloud head, part of which is itself considered to be due to moist air flowing slantwise above the low-θ_w air associated with CF2. The more irregular nature of the cloud band along CF2 compared with the smooth texture of that ahead of CF1 is due to the lower air temperatures which led to the CF2 cloud being more convective. Even so, the associated cloud tops were no higher than 1.5 km (dark green band along CF2 in Fig 8). Behind CF2 the linear nature of the cold frontal cloud gave way to irregular open cellular convection typical of subsided arctic airflows over a relatively warm sea. The sea surface temperatures in the frontal region

were between 11 and 13C, leading to a significantly unstable boundary layer behind CF1 but a near neutrally stable boundary layer in the warm sector ahead of CF1 where dry and wet bulb temperatures, at 12 to 13°C, were virtually equal to the sea surface temperature.

(d) Visualization of the flows associated with CF1, CF2 and the cloud head

The flow of cold air associated with CF1 and CF2 was interrupted by the interleaving of the flow of moister air circulating rearwards in the southwestern tip of the cloud head. The latter is the rearward-sloping ascent above the cold air of CF2. Before examining the two cold frontal flows we shall first consider this cloud head flow, as represented in Fig 9 (a). To establish a visual link between this figure and other parts of Fig 9 (and 8) we have shaded the region of the cloud head where the moist layer (RH>90%), derived from the dropsondes, extended above 1.5 km. Reference to the infra-red image in Fig 8 shows that both this contour and the 3 km contour are consistent with the satellite cloud top pattern (except to the southwest of Brittany where the cloud head moisture boundary was obscured by much higher cloud associated with the polar front cloud band).

We now consider the cloud head flow in detail. On the right side of Fig 9(a) the dot-dashed contour shows the location of a shallow layer of rather dry air (RH<90%) whose base was at 0.5 km. This corresponded to the air (with θ = 13C) within the CCB ahead of the warm front that subsequently entered the cloud head. The streamlines in Fig 9(a) show this flow rising towards the northwest, with its relative humidity increasing to 100%. The subsequent saturated flow is plotted within the θ_w = 7C surface which shows the CCB flow eventually emerging at the tip of the cloud head at between 1 and 2 km. This was the flow that was interleaved between the cold flows approaching cold fronts CF1 and CF2.

The airflows that penetrated close to the surface just behind CF1 and CF2 are represented in Figs 9(b) and 9(c) by the relative flows in the θ = 20 and 10C surfaces, respectively. The θ = 20C flow in Fig 9(b) can be seen descending steeply from the nor-northwest, part of it overrunning the tip of the cloud head. By the time it reached the position of CF1 it was at 1.5 km and turning towards the northeast. Mixing processes are believed to have brought some of this air down to the ground and, indeed, the dropsondes showed that in the diagonally hatched area in Fig 9(b) the RH=90% contour dropped as low as 0.5 km indicating strong downward penetration of the cold dry air along this part of CF1. As far as the CF2 flow in Fig 9(c) is concerned, the θ = 10C flow shown here is near the boundary layer and so the analysis can be relied upon in only a semi-quantitative sense; however, it suggests that the flow was descending to reach the surface just behind CF2. Parts of the flow can be seen undercutting the tip of the cloud head.

4. Evolution of the cold fronts

(a) The dry intrusions associated with CF1 and CF2.

Fig 10 shows a 3-hourly sequence of water vapour imagery, with the position of surface cold fronts CF1 and CF2 superimposed. The WV imagery, which indicates the pattern of water vapour in the middle and upper troposphere, shows dark zones due to two dry intrusions corresponding to the two surface fronts. The first dry intrusion straddles CF1. The second dry intrusion lies immediately behind CF2. The dark zone associated with the latter dry intrusion was growing in extent presumably in association with descent over a deep layer. However, the dark zone associated with the first dry intrusion diminished in extent, becoming quite narrow by the end of the period. This is thought to have been partly because

of stretching deformation and partly because it was within the region where the dry intrusion air was turning towards the northeast and ascending above a moist zone. Such a behaviour is consistent with the evolution of CF1 as diagnosed below.

(b) Transition of CF1 from a surface cold front to an upper cold front.

Fig 11 shows part of the surface analysis and associated cloud heads for two times 9 hours apart. The first analysis corresponds to the dropsonde analysis discussed in Sec 3. The second analysis, based mainly on reports over France and the UK, shows an interesting change in structure: whereas CF1 and CF2 were both diagnosed as surface fronts at 18 UT, CF1 had become an upper cold front by the later time. No corresponding wind change or temperature change occurred at the surface with the passage of CF1 over stations such as Jersey. Indeed at the time of the passage of CF1 over Jersey the surface temperature and dew point were still increasing and continued to increase for some time. Meanwhile CF2, which previously had been over 100 km behind the warmest surface air, had come right up to the edge of the warm sector to become the main surface cold front.

Evidently, the two cold fronts were travelling faster than the rest of the system, where we define the rest of the system as being the combination of the cloud head, low centre and the belt of 'warm sector' air with highest θ_w. The motion of the cold fronts was related to the higher velocity of the air in the overrunning dry intrusions. The warm sector was situated within a region of ascent ahead of the trough and, as the dry intrusions approached, the formerly descending dry air ascended and overran the high-θ_w air in the warm sector. Thus by the later time (28 April/03 UT) the region between CF1 and CF2 was characterized

by a shallow moist zone (SMZ) overlain by dry air as in the split front model of Browning and Monk (1982). Infra-red satellite imagery showed that the cloud tops were very low (between 1 and 3 km) in the SMZ. At this stage the reader will recognize similarities to the simple conceptual model in Fig 1 where the leading edge of the overrunning dry intrusion is depicted as an upper cold front (open cold front symbols).

(c) Middle-level convection along the upper cold front.

A radiosonde was released at 23 UT from Brest at the leading edge of the SMZ close to the position of the upper cold front, CF1. It shows significant middle tropospheric potential (and actual) instability (Fig 12), consistent with the occurrence of the relatively deep convective clouds observed along CF1 a few kilometres to the north of Brest (Fig 13). Fig. 13 shows hourly plots of CF1 and the clouds along it as it approached the Brest area. Most of the tops were below 3 km (about -5C) but near the cyclone centre they extended above 6.5 km (colder than -30C). The convective cells formed a short line, each cell developing at the southern end and dissipating after a few hours at the northern end. Fig 13 shows that the lifting was sufficient to realise the mid-level instability only within 100 km of the surface low.

In order to keep Fig 13 simple we have not shown the high cloud tops that developed before 16 UT and were located at the northern end of CF1 for a while after 16 UT. They behaved just like the other convective cells described above, but further insight into their origin is provided by the dropsondes that were released between 1430 and 1530 UT during Run 3 (see Fig 3). This run was almost parallel to CF1 and a little ahead of it. Its position

with respect to the near-surface fronts can be seen in Fig 6 where Run 3 is the line of numbers extending from the underlined 8 ahead of the warm front to the underlined 12 within the warm sector just ahead of CF1. A vertical cross-section of θ_w along this line is shown in Fig 14. The most obvious feature of Fig 14 is the inclined warm frontal zone reaching the surface half-way along the section. However, it also shows two features that are related to CF1 and the associated mid-level convection. The feature related to CF1 is the layer of low-θ_w air between 2 and 3 km (labelled CC in Fig 14) intruding above the high-θ_w warm-sector air. This intrusion of low-θ_w air corresponds to the dry air in the 25C θ-surface that was overrunning CF1 as shown in Fig 5. It produced the shallow layer of potential instability that was realised in the region of ascent close to the low centre where this air began to overrun the warm frontal zone (see schematic cloud turret in Fig 14).

Fig 15 shows the weather radar rainfall pattern at 28 April/01 UT superimposed on the Meteosat infra-red image at a late stage in the evolution of CF1. The convective clouds associated with the upper cold front CF1 gave rise to moderate rain showers in a roughly south-north line from Cherbourg to central southern England. Consistent with the lowering of tops of the deepest convection from 27th/22 UT onwards (Fig 13), the rain showers were weakening at this time as CF1 travelled eastwards away from the low centre. The main area of rain to the west of this line, associated with the cloud head, subsequently travelled over the highly sensitive Doppler radar at Chilbolton (southern England). This and other land-based data have been used to validate NWP model runs at different resolutions, initialized with and without dropsondes. This study is reported elsewhere (Ballard et al 1995).

5. Vertical structure of the dry intrusions penetrating into the low troposphere

This section is based upon detailed analyses of dropsoundings during Run 5 which provided a cross-section roughly north-south through the southwestern tip of the cloud head (see location of Run 5 in Fig 3). There were two levels of complexity in the observed structure. We start, in Sec 5(a), by drawing attention to the primary double structure associated with the two dry intrusions and cold fronts CF1 and CF2. Then in Secs 5(b) and (c), respectively, we describe and then try to account for some coherent structures occurring on an even finer scale.

(a) The primary features of the vertical structure associated with CF1 and CF2

The two dry intrusions and the two associated cold fronts show up well in the fields of relative humidity and θ_w reproduced in Figs 16 and 17. Although there is a lot of fine structure (discussed later) this does not obscure the two main thrusts of dry low-θ_w air that are situated on different sides of the tip of the cloud head (see large arrows labelled 1 and 2 in Fig 17). The features of the θ_w-pattern that relate most clearly to the double frontal structure are:

- *Dry Intrusion 1.* The overrunning flow of air above the cloud head, with a region of θ_w between 9 and 11C descending toward the surface in advance of the cloud head but behind the cloud that was associated with CF1. This flow was subsaturated and corresponds roughly to the air with θ=20C as analysed in Fig 9(b).
- *Dry Intrusion 2.* Air with low θ_w, between 4 and 6C, extending to the surface behind CF2 which was itself marked by a locally sharp θ_w-gradient. This air was initially subsaturated and corresponds roughly to the flow of air

with θ=10C that was analysed in Fig 9(c);

- *Cloud Head* . Air with θ_w between 6 and 9C, associated with the cloud head itself. This corresponds to the flow of air that was analysed in Fig 9(a). Much of the cloud material within the part of the cloud head observed in Run 5 was formed by ascent that occurred in the main part of the cloud head to the northeast of Run 5. As discussed in Sec. 3(b), it is not clear exactly what the vertical air motion was in the tip of the cloud head. Probably the best way of thinking of it is that this was a cloudy region of near-zero vertical velocity slicing into the region of otherwise descending air associated with the dry intrusions.

(b) Additional fine-scale structure within the dry intrusions.

In addition to the broad features just discussed, Figs 16 and 17 show a considerable amount of finer-scale structure, especially just above and in advance of the cloud head. This sub-structure is seen as inclined thin fingers. Corresponding fingers are evident in another vertical section farther west (Run 6, not shown) and so the fingers were evidently sections through inclined laminae. These laminae show up especially clearly in the pattern of relative humidity depicted on Fig 16 (see the multiple dashed lines). Note that both Figs 16 and 17 have been derived subjectively specifically to reveal these laminae, which were found to be inadequately resolved in objective analyses. A typical vertical spacing between successive dry laminae within a given dry intrusion is 1 km. The component of their slopes within the observed section was about 1 in 100. Allowing for the fact that the line of

soundings cut obliquely across the cold frontal zone, the true slope of the laminae was about 1 in 60 and their horizontal spacing 60 km.

One particularly well defined dry lamina, located just above the cloud head, can be seen in Fig 16 extending for over 200 km in the horizontal and 2 km in the vertical. It was resolved in four consecutive dropsonde profiles, two of which are shown in Fig 18. The overlying moist lamina was just as extensive as its dry counterpart and although its maximum humidity often exceeded 80% it did not (quite) reach saturation above 1 km. This is consistent with the infra-red imagery which showed that, apart from the narrow line of cloud below 1 km, there was no cloud between the cloud band associated with CF1 (labelled C1 in Fig 16) and the main cloud head.

Figure 19 shows that the first dry intrusion, which brought dry low-θ_w air down ahead of the cloud head, was associated with an inclined lamina of strong vertical shear in the component of the wind parallel to the cold fronts. Below 3 km this was split into several thinner laminae. The three best defined laminae in Fig 19 are seen to have corresponded closely to the independently measured relative humidity laminae in Fig 16. The dashed curve in Fig 19 shows that these laminae lay within a region where the component of the wind resolved along the direction of travel of the large-scale system was close to the system velocity. The possible significance of this is discussed next.

(c) Possible mechanisms to account for the fine structure

Figs 20(a) and 20(b) show objectively analysed cross-sections of potential vorticity

(PV) and equivalent PV (hereafter referred to as EPV - Thorpe and Clough, 1991) deduced from the dropsonde observations along Run 5. Although these quantities are noisy on the mesoscale, we believe they nevertheless display some significant features. In particular, some low values of PV and EPV are indicated, especially in the dry air overlying the cloud head. Manual analyses of the observations are consistent with this, showing both low vorticity and low static stability in this region. The fact that much of this low PV occurred within the dry air suggests that this part of the fine structure was not induced by diabatic processes occurring recently in the system but, rather, that it results from descent of air that already possessed low PV. We are more accustomed to thinking in terms of dry intrusions bringing down high-PV air from tropopause level (eg Browning and Reynolds 1994); however, in the vicinity of a tropopause fold, the flow of stratospheric air with high PV is contiguous with a flow of tropospheric air of low, and sometimes even negative, PV or EPV caused by previous latent heat release upstream. Presumably it is the descent of this latter air that characterises parts of the dry intrusion shown in Fig 20. According to semi-geostrophic theory the response of the vertical velocity to geostrophic forcing is given by an appropriate omega equation, in which the role of potential vorticity resembles that of static stability (Hoskins and Draghici 1977). Thus it is clear qualitatively that, for an equal forcing of descent, the air with low PV will descend by more than the adjacent stratospheric air; this is consistent with the observed structure.

The regions of negative PV and EPV are suggestive of the presence of symmetric instability (SI) or conditional symmetric instability (CSI). Also, the two-fold vorticity pattern resembles symmetrically unstable circulations as simulated in two dimensions by Thorpe and

Rotunno (1989). However, for most of their simulations the domains were initially unstable throughout, whereas in this case the areas of negative PV (Fig 20(a)) are quite limited in extent and primarily in dry air (as in Thorpe and Cloughs' IOP 7 case). The regions of negative EPV in Fig 20(b) are somewhat more extensive but the regions of strongly negative EPV occur mainly just above the cloud (see 95% relative humidity contour in Fig 20(b)) rather than in it. We are therefore inclined to doubt that SI or CSI alone can provide a complete explanation of the multiple laminae. The evidence at the end of Sec 5(b) is that the multiple laminae occurred in a region that was near-critical with respect to the frontal wave; this has no significance in the context of an unstable growth mechanism such as SI or CSI but it does suggest another possibility.

Critical layer effects occur in parcels of air that move at the same velocity as a wave in which a forcing process operates; such parcels are subjected to protracted forcing and will thus show the results of forcing more intensely than those at other locations in the fluid. We are not aware of any observational studies highlighting such processes, but their importance has been noted by Hoskins and West (1979) and Davies et al (1991) in the context of theoretical studies of frontogenesis. Both of these studies considered the formation of fronts in dry 3-dimensional semi-geostrophic models of baroclinic wave development. Hoskins and West (1979) demonstrated that the greatest frontogenesis occurred where parcel trajectories stayed longer within the region of intense frontogenesis, while Davies et al (1991) showed that frontogenesis in differing basic state flows was most pronounced in regions of the fluid moving close to the phase velocity of the unstable baroclinic mode. The forcing process in the models was purely ageostrophic motion, and this appears likely also

in the case considered here. In general, however, forcing might also be due to diabatic processes if these have a fixed or slowly varying phase relative to the wave (Lin and Chun 1991). They may thus be expected to "etch" out a pattern with scale and intensity determined not only by the extent and strength of forcing but also by the duration implied by the system-relative velocity. Note, however, that since the speed of a wave changes as it develops, the critical region will differ with time, probably tending to descend as a wave decelerates during growth.

In the present study much of the fine-scale structure occurred at heights between 1 and 3 km, close to the edge of the moist boundary layer, and so it is possible that latent heating had some influence on the fine-scale structure. This influence may have been exercised primarily by determining the local stability, thereby increasing the amplitude of the secondary response to the forcing perturbation.

In summary, low PV, or EPV, is seen to have been important for the development of the fine structure in this case, but the viewpoint adopted here is different to the conventional view that such structure is determined mainly by local instabilities such as CSI. Our suggestion is, firstly, that the externally imposed baroclinic wave phase speed is a primary influence and, secondly, that the importance of local stability may arise in determining the amplitude of response to an imposed forcing (such as divergence of the Q vector) rather than by implying a spontaneously unstable growth.

6. Conclusions

We have presented a case study of a moderately rapidly developing frontal cyclone which displayed a characteristic structure comprising cloud head and dry intrusion - in this case actually two dry intrusions in close succession. Most frontal cyclones contain a dry intrusion(s), which is the specific name given to the region of dry, low-θ_w air that enters the cyclone system from the near following a period of descent from near a tropopause fold. In this study we have made use of an unusually dense array of soundings to focus on the structure of the dry intrusions and on the way in which they interacted with the cloudy air both ahead of them and in the cloud head.

The double structure of the dry intrusion was manifested aloft as two distinct dry slots (dark zones) in the satellite water vapour imagery and, at the surface, as two cold fronts 100 to 200 km apart. The dry intrusions travelled faster than the cyclone system and, over the period of the study, the leading dry intrusion advanced ahead of the cyclone centre. As it did so, it did not displace the warm-sector air and lead to a process of occlusion as in the Norwegian model. Instead it rode over the shallow moist zone of high-θ_w air in the warm sector, whilst the latter continued to feed boundary-layer air into the cloud head to the north of the cyclone centre. The first cold front thus became an upper front, and the second cold front then took its place as the new surface boundary of the warm sector. This is evidently one of the ways in which the split-front structure in the model of Browning and Monk (1982) can develop. Presumably a similar process could occur even in the absence of a double dry intrusion, in association with different parts of a single dry intrusion, ie when just the leading edge overruns the warm sector.

The surface cold fronts in the present study were characterised by thin lines of shallow stratocumulus that extended southwestwards from the cyclone centre. Evidently they were kata-fronts and they produced hardly any precipitation. When the first cold front rode over the shallow moist zone (warm sector) and developed into an upper front, a line of mid-level convective shower cells formed along it. The showers were confined to a short line within 100 km of the cyclone centre where there was sufficient lifting above the warm front to realise the potential instability.

The main precipitation region of the cyclone was associated with the cloud head located mainly to the north of the cold fronts. This is the region where cold conveyor belt air and warmer air from the base of the warm conveyor belt combined to give an area of rearward-sloping ascent to the north of the cyclone centre as in the model of Browning and Roberts (1994). The stratiform cloud deck that composed the present cloud head reached above 6 km over a large area but the main focus of this study was on the southwestern tip of the cloud head where the cloud top was below 3 km. Here, cloud that had formed during previous ascent within the main part of the cloud head, was travelling southwestwards relative to the system and becoming interleaved between the two dry intrusions.

The region where this interleaving occurred, west of the cyclone centre, was characterised by considerable fine structure. Inclined sheets of strong shear and cyclonic vorticity, associated with the edge of one of the dry intrusions, split into multiple inclined laminae near the top of the boundary layer at heights of between 1 and 3 km. Our detailed observations provide an interesting glimpse of the ordered and highly laminar interactions that occur where the descending air within dry intrusions encounters the moist boundary layer.

The multiple layered structure was revealed not only in the kinematic fields but also in the independently-measured fields of relative humidity and wet-bulb potential temperature because of the distortion of the boundary-layer top by the localised shears. Individual moist and dry laminae were inclined at an angle of 1 in 60 with a spacing between successive moist laminae of about 60 km. The moist laminae corresponded to air from the boundary layer and the dry laminae corresponded to the dry-intrusion air penetrating slantwise into the boundary layer.

The laminated fine structure resembles that expected from conditional symmetric instability and, indeed, there were pockets of small and even negative potential vorticity and equivalent PV. It is not clear, however, that the extent of these pockets was sufficient to account fully for the observed fine structure. The fine structure occurred close to the critical level of zero wind velocity relative to the cyclone system, and so it may simply have been a response to sustained ageostrophic forcing of the same parcels of air. Whatever its cause, the existence of the fine structure sheds new light on the nature of the mixing processes that sometimes occur at the top of the boundary layer. We suspect that this kind of structure is common in the regions just upwind of developing cloud heads where it leads to the multiple shallow cloud lines often seen in satellite visible and infra-red imagery.

References

Browning, K.A. and Monk, G.A. 1982 A simple model for the synoptic analysis of cold fronts. Q.J.R.Meteorol. Soc., 108, 435-452.

Browning, K.A. and Reynolds, R. 1994 Diagnostic study of a narrow cold-frontal rainband and severe winds associated with a stratospheric intrusion. Q.J.R.Meteorol.Soc., 120, 235-257

Browning, K.A. and Roberts, N.M. 1994 Structure of a frontal cyclone. Q.J.R.Meteorol.Soc., 120, xxx-xxx.

Davies, H.C., Schär, C. and Wernli, H. 1994 The palette of fronts and cyclones within a baroclinic wave development. J.Atmos.Sci., 48, 1666-1689.

Hewson, T.D. 1993 The Fronts 92 Experiment: a Quicklook Atlas. JCMM Internal Report No 15, 176pp. Available from the Meteorological Office Library.

Hoskins, B.J. and Draghici, I. 1977 The forcing of vertical motion according to the semi-geostrophic equations and in an isentropic co-ordinate model. J.Atmos. Sci., 34, 1859-1867.

Hoskins, B.J. and West, N, 1979 Baroclinic waves and frontogenesis. Part II: uniform potential vorticity jet flows - cold and warm fronts. J.Atmos. Sci., 36, 1663-1680.

Lin, Y.H. and Chun, H-Y 1991 Effects of diabatic cooling in a shear flow with a critical level. J.Atmos.Sci., 48, 2476-2491.

Pedder, M.A. 1993 Interpolation and filtering of spatial observations using successive corrections and Gaussian filters. Mon.Wea.Rev., 121, 2889-2902.

Thiebaux, H.J. and Pedder. M.A. 1987 Spatial objective analysis with applications in atmospheric science. Academic Press, 295 pp.

Thorpe, A.J. and Clough, S.A. 1991 Mesoscale dynamics of cold fronts: Structures described by dropsoundings in FRONTS 87. Q.J.R.Meteorol. Soc., 117, 903-941.

Thorpe. A.J. and Rotunno, R. 1989 Nonlinear aspects of symmetric instability. J.Atmos. Sci., 46, 1285-1299.

FIGURE LEGENDS

Fig 1. Conceptual model showing the intertwining around the low centre (L) of two rather symmetrical flows: (a) the dry intrusion and (b) the cloud head flow. The cloud head flow consists of cold conveyor belt air and air from the base of the warm conveyor belt (the main part of the warm conveyor belt flow, associated with the polar frontal cloud band, is not shown here). Based on Browning and Roberts (1994).

Fig 2. Outlines of satellite cloud head (cloud top temperature <-15C) superimposed on positions of low centre (L) at 6-h intervals from 18 UT on 26 April to 06 UT, 28 April 1992. Full satellite IR image for 18 UT, 27 April is shown on right, with a cloud top temperature grey scale beneath it.

Fig 3. Times and locations of dropsondes during FRONTS-92 IOP3 on 27 April 1992. Numbers show the time (UT) when the sonde was about half way between the level of release and the sea surface (this was about 5 min after the sonde was released). Locations of the sondes are adjusted to their positions relative to the system at 18 UT.

Fig 4. Surface and cloud analysis for 18 UT, 27 April. See text for details.

Fig 5. Visualization of the broad 3-D pattern of airflow in and near the cloud head at 18 UT, 27 April obtained from relative-flow analyses in three isentropic surfaces. Thick solid and thick open streamlines show flow in the 12C and 8C θ_w-surfaces, respectively. Thin solid streamlines show flow in the 25C θ-surface. Dashed and dotted lines show heights of these three surfaces at 1 km intervals. Stippled shading represents saturated flows and dashed shading denotes relative humidity less than 30% within the corresponding isentropic surfaces. Area of figures corresponds exactly to that of Fig 4. Other details in text.

Fig 6. 950-mb distribution of θ_w for 18 UT, 27 April, derived from a subjective analysis of the dropsondes. Isopleths are labelled with large numbers (degC). The small numbers show the θ_w-values for individual soundings displaced according to the system velocity. The tip of the warm sector/low centre was determined by a ship observation.

Fig 7. Meteosat visible imagery for 1730 UT, 27 April showing the well-defined clearance of cloud (thin black strip) immediately behind CF1.

Fig 8. Meteosat infra-red false-colour imagery for 18 UT, 27 April with surface frontal positions taken from Fig 6. Cloud top temperatures are given by the colour code along the bottom. Also shown are isopleths of the depth of the moist (90% RH) layer deduced from the dropsondes.

Fig 9. System-relative flows of (a) moist air in the θ_w = 7C surface within the cloud head, (b) dry air in the θ = 20C surface just behind CF1 and (c) dry air in the θ = 10C surface just behind CF2. Part of the flow in (a) intrudes between the flows in (b) and (c). Dashed lines show the heights of these surfaces. Dotted lines show relative humidity. Also shown are the position of the low centre (L) and extent of moist air (RH>90%) above 1.5 km associated with the cloud head (stippled shading). The 0.5 km base of a shallow layer of dry air beneath the warm frontal zone is denoted by the dot-dashed isopleth in (a). Another region where dry air penetrated downwards as far as 0.5 km is shown in (b) by hatched shading.

Fig 10. Sequence of Meteosat water vapour images at (a) 1230, (b) 1530, (c) 1830 and (d) 2130 UT, 27 April. Dark areas correspond to dry mid- and upper-tropospheric air. The lightest areas correspond to cloud (the cloud head occupies the top right quarter of the image). The area is displaced according to the system velocity to keep the cold fronts (solid lines) within the field of view.

Fig 11. Frontal analyses at 18 UT, 27 April and 03 UT, 28 April, together with the corresponding analyses of surface wet bulb temperature (950 mb θ_w in the case of the 18 UT analysis). Shaded areas show the locations of the southwestern portion of cloud head (-15C cloud top). The thick line over the Channel, continuous with CF2, corresponds to the southernmost rainband associated with the cloud head. L denotes the low centre. J shows the location of Jersey.

Fig 12. Tephigram showing temperature and dewpoint sounding from Brest at 23 UT, 27 April. See Fig 13 for location.

Fig 13. Evolution of convective clouds associated with CF1 that developed after 16 UT. The successive hourly positions of cloud tops have been derived from Meteosat IR imagery. Stippled and hatched shading denotes tops colder than -5C and -30C, respectively. Short arrows show tracks of individual cloud elements. Hourly positions of CF1 are also indicated. The track of the surface low was between XX. B denotes the location of the Brest ascent plotted in Fig 12.

Fig 14. Cross-section along Run 3 within the warm sector just ahead of CF1 (see location in Figs 3 and 6), showing pattern of θ_w (isopleths at 0.5C intervals) derived objectively from the dropsondes. Locations of the 10 dropsondes are shown at the top of the diagram. The bold solid line demarcates the region of strong convergence ($>4x10^{-5}s^{-1}$) associated with the warm frontal zone. The dashed line labelled CC shows the intrusion of relatively dry low-θ_w air overrunning the moist warm sector air ahead of CF1. The schematic cloud turret shows the observed location of middle-level convection.

Fig 15. Distribution of rain from the UK weather radar network superimposed on the IR imagery from Meteosat for 01 UT, 28 April. Rainfall rates (mm h^{-1}) and cloud top temperatures (degC) are given by the colour codes at the top and

bottom, respectively. There are two main areas of rain in the cloud head region (rain associated with the polar front cloud band over France is not shown). The band of rain stretching northwards from Cherbourg to central southern England was associated with mid-level convection along the upper-level cold front, CF1. The larger area farther west was associated with the main region of slantwise ascent within the cloud head. The southern part of the latter area was also convective, especially close to the southern tip of the cloud head near CF2, where it was overrun by the dry intrusion.

Fig 16. Cross-section along Run 5 (see location in Fig 3) showing isopleths of relative humidity derived subjectively from dropsondes, superimposed upon the outline of cloud tops derived from infra-red imagery. Locations of the 17 dropsondes are shown at the top of the diagram.

Fig 17. Same as Fig 16 but showing isopleths of θ_w instead of relative humidity. The large arrows labelled 1 and 2 draw attention to the two dry intrusions with low θ_w associated with Cold Fronts 1 and 2.

Fig 18. Two adjacent dropsonde profiles along Run 5 showing the moist and dry laminae just above the moist air associated with the southwestern tip of the cloud head. Their locations are shown in Fig 3: (a) and (b) reached mid-flight at 1700 and 1706, respectively.

Fig 19. Same as Fig 16 but showing the vertical shear in the component of the wind resolved parallel to the cold fronts (stippled laminae show shear greater than 1 ms^{-1} per 100 m). Also shown (dashed curve) is where the component of the wind resolved along the direction of travel of the cyclone system was equal to the system velocity.

Fig 20. Cross-sections along Run 5 (see location in Fig 3) showing patterns of (a) dry potential vorticity (PV) and (b) equivalent potential vorticity (EPV) derived objectively from the 17 dropsondes neglecting the contribution to PV due to the component of horizonal wind shear parallel to the section. Isopleths are at intervals of 0.5 and 1 PV unit in (a) and (b), respectively; areas that are positive are stippled. Also shown, by the heavy contour, is the subjectively analysed extent of moist air with relative humidity in excess of 95%.

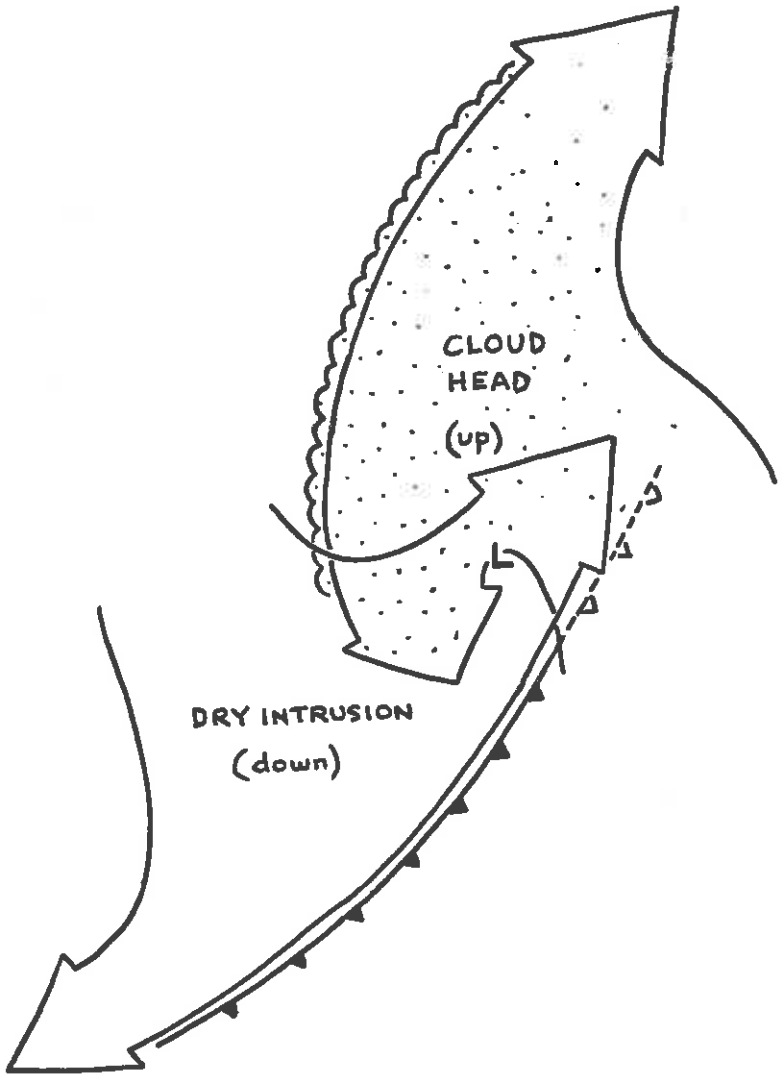

Fig 1

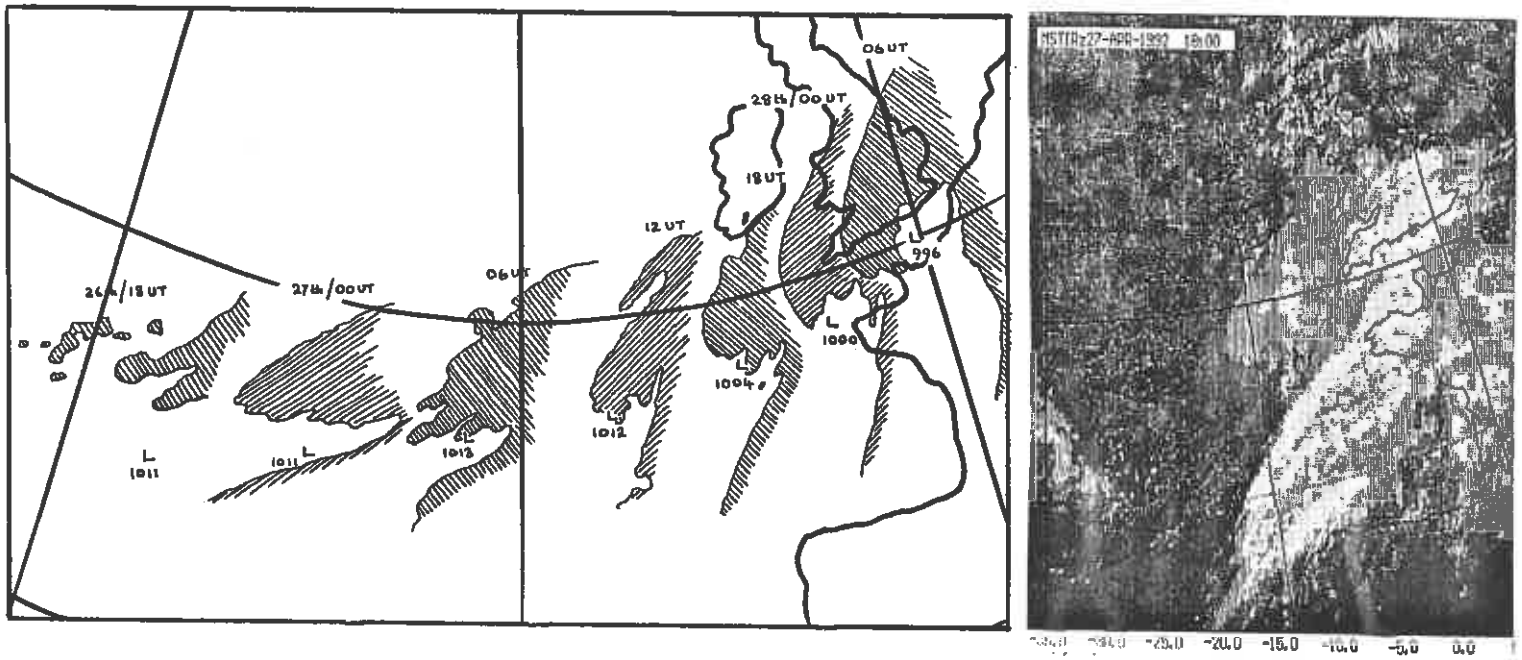
06 UT
28/00 UT
18 UT
12 UT
06 UT
27/00 UT
26/18 UT
L
996
L
1000
L
1004
L
1012
L
1012
L
1011
L
1011
NOAA12-27-APR-1992 19:00
-25.0
-20.0
-15.0
-10.0
-5.0
0.0

Fig. 2

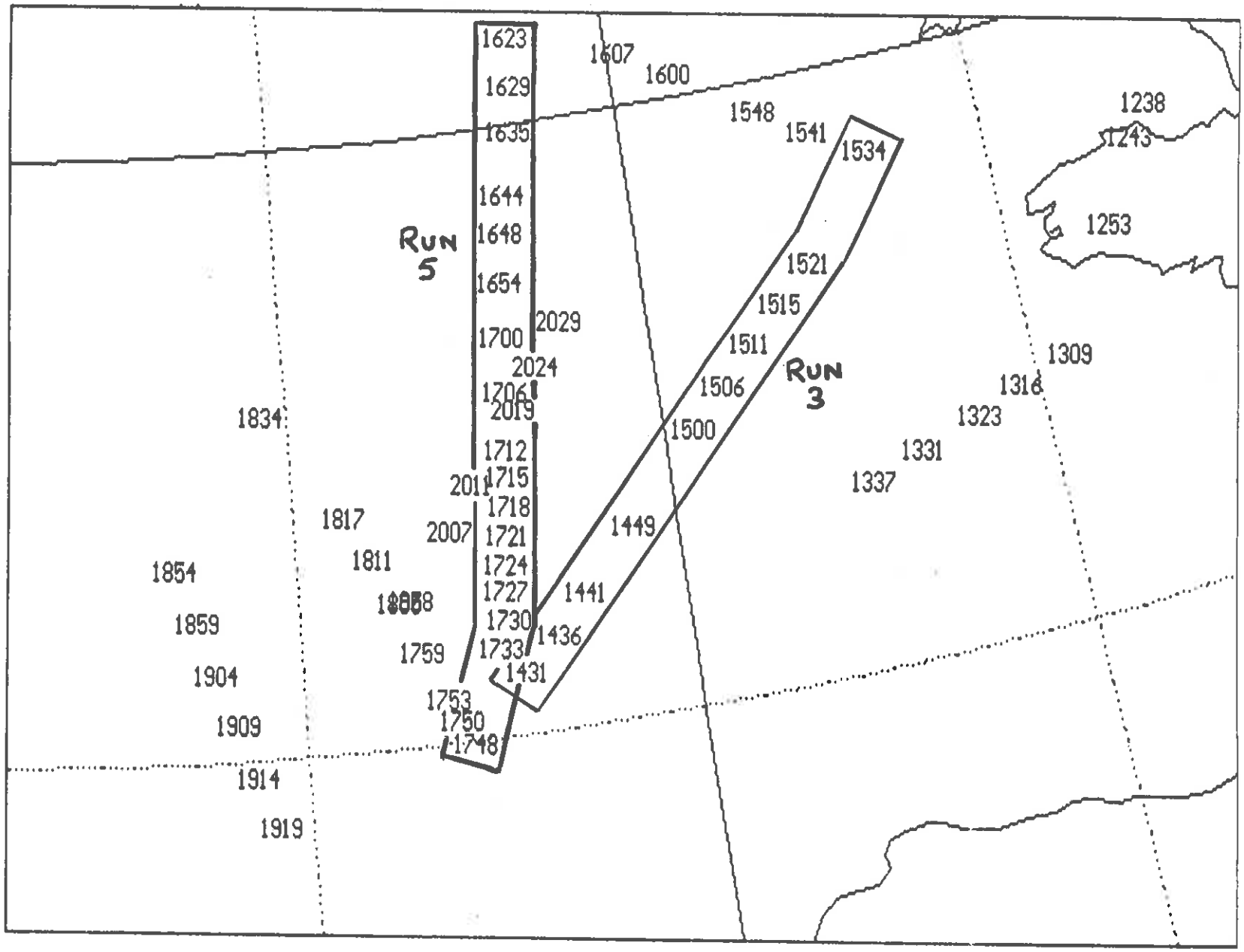
1623
1629
1635
1644
1648
1654
1700
2029
2024
1706
2019
1712
1715
2011
1718
1721
2007
1724
1727
1730
1733
1759
1753
1750
1748
1607
1600
1548
1541
1534
1521
1515
1511
1506
1500
1449
1441
1436
1431
RUN 5
RUN 3
1238
1243
1253
1309
1316
1323
1331
1337
1834
1817
1811
1854
1859
1904
1909
1914
1919

Fig 3

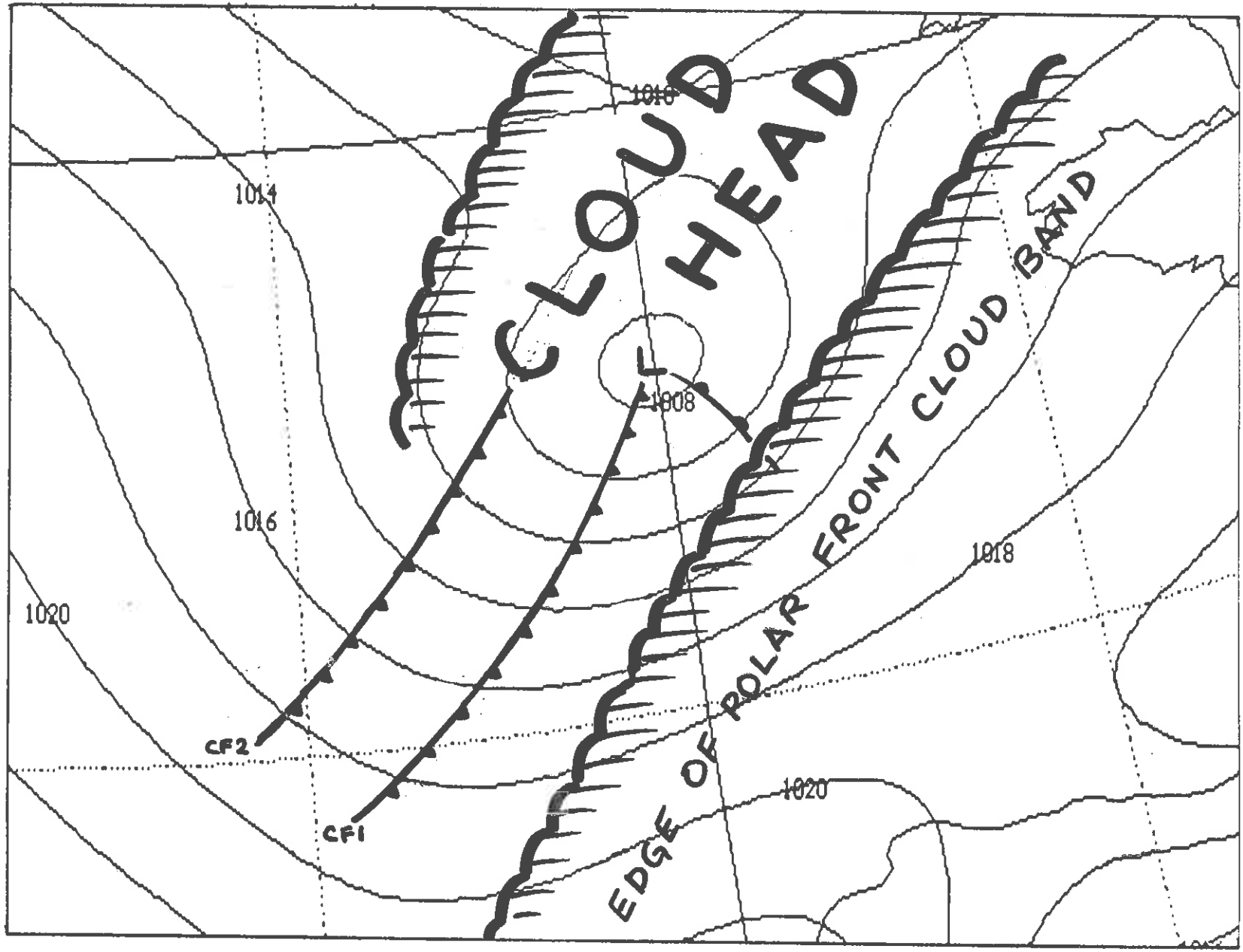
CLOUD HEAD
EDGE OF POLAR FRONT CLOUD BAND
1014
1016
1008
1016
1018
1020
1020
CF2
CF1

Fig 4

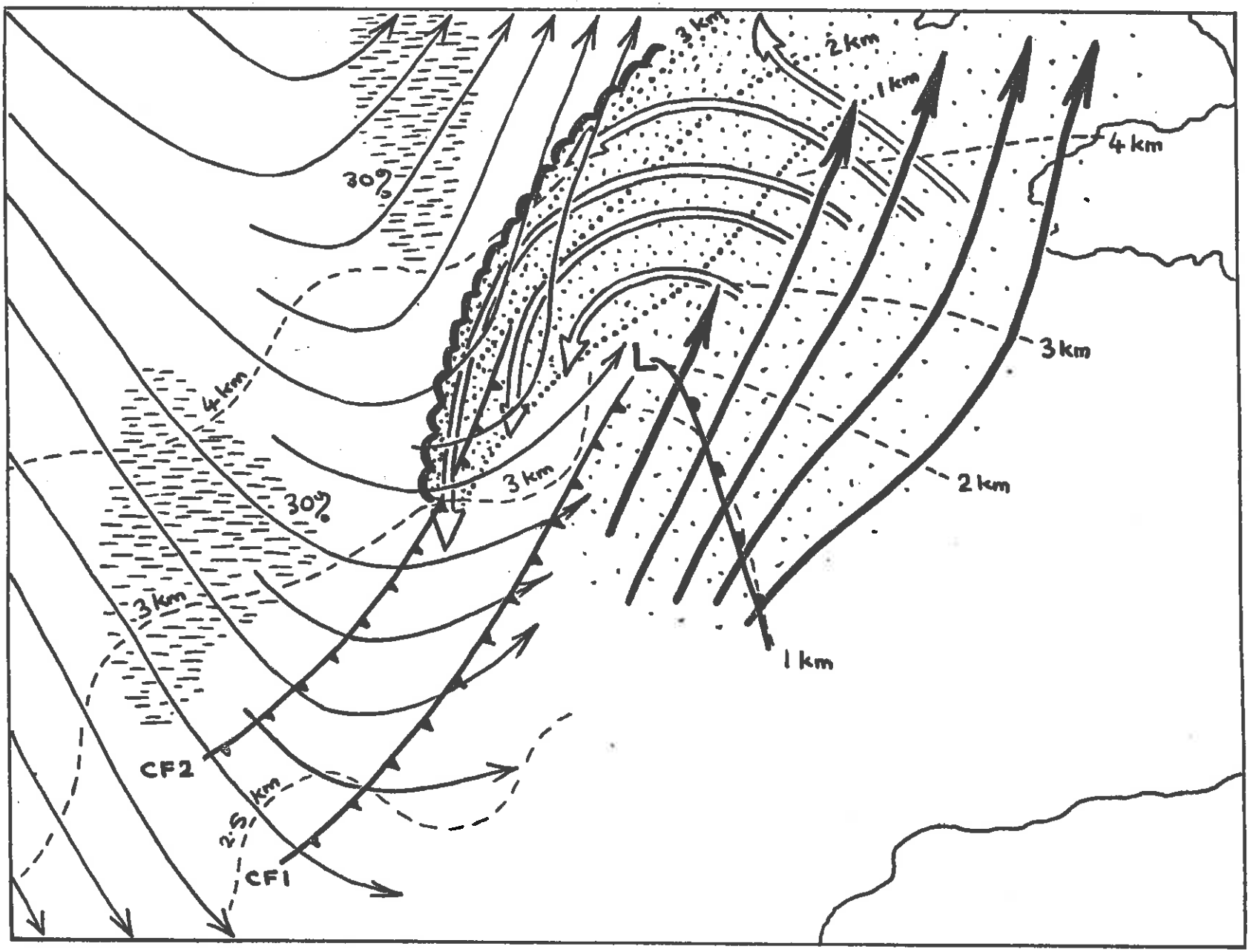

Fig 5

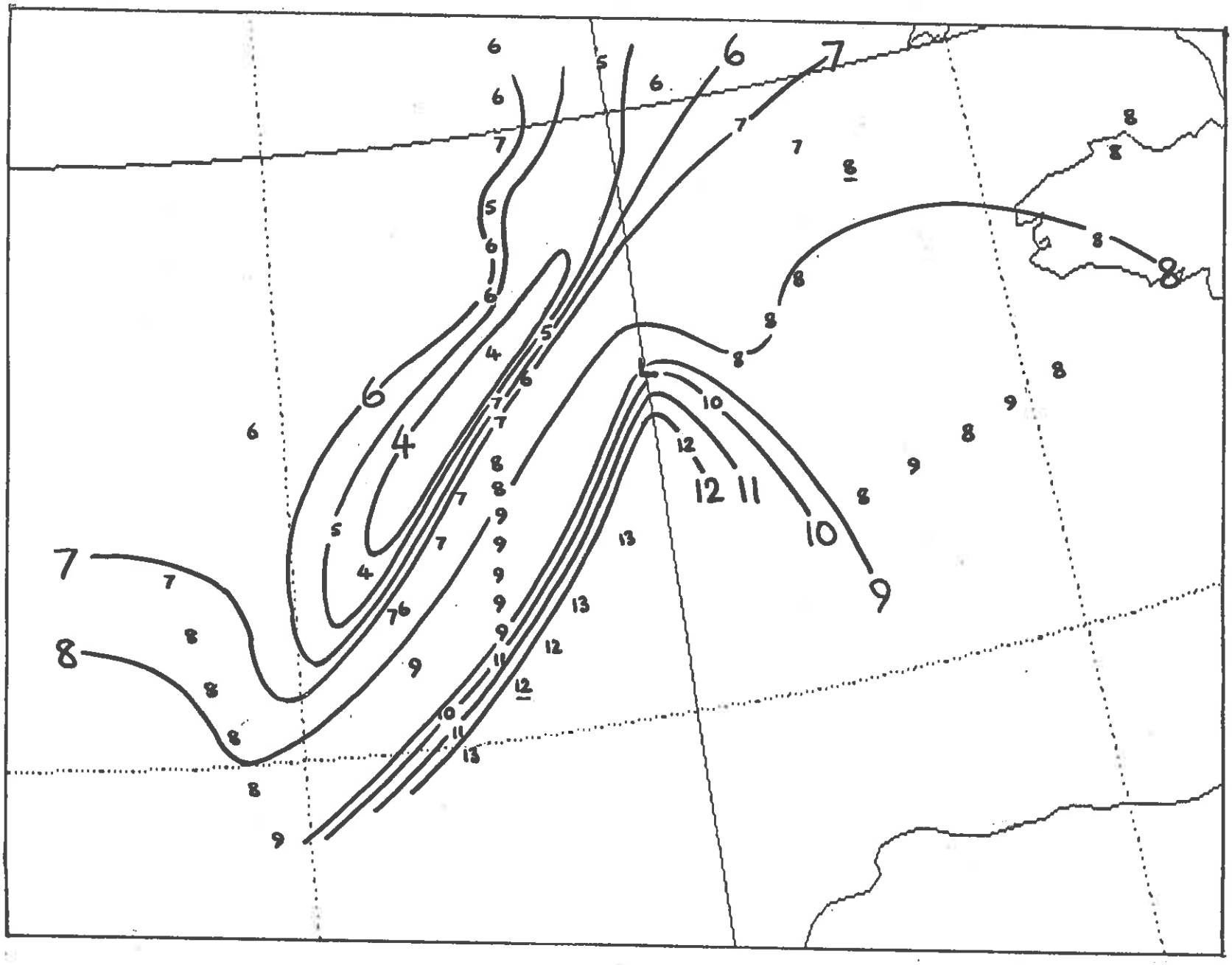

Fig 6

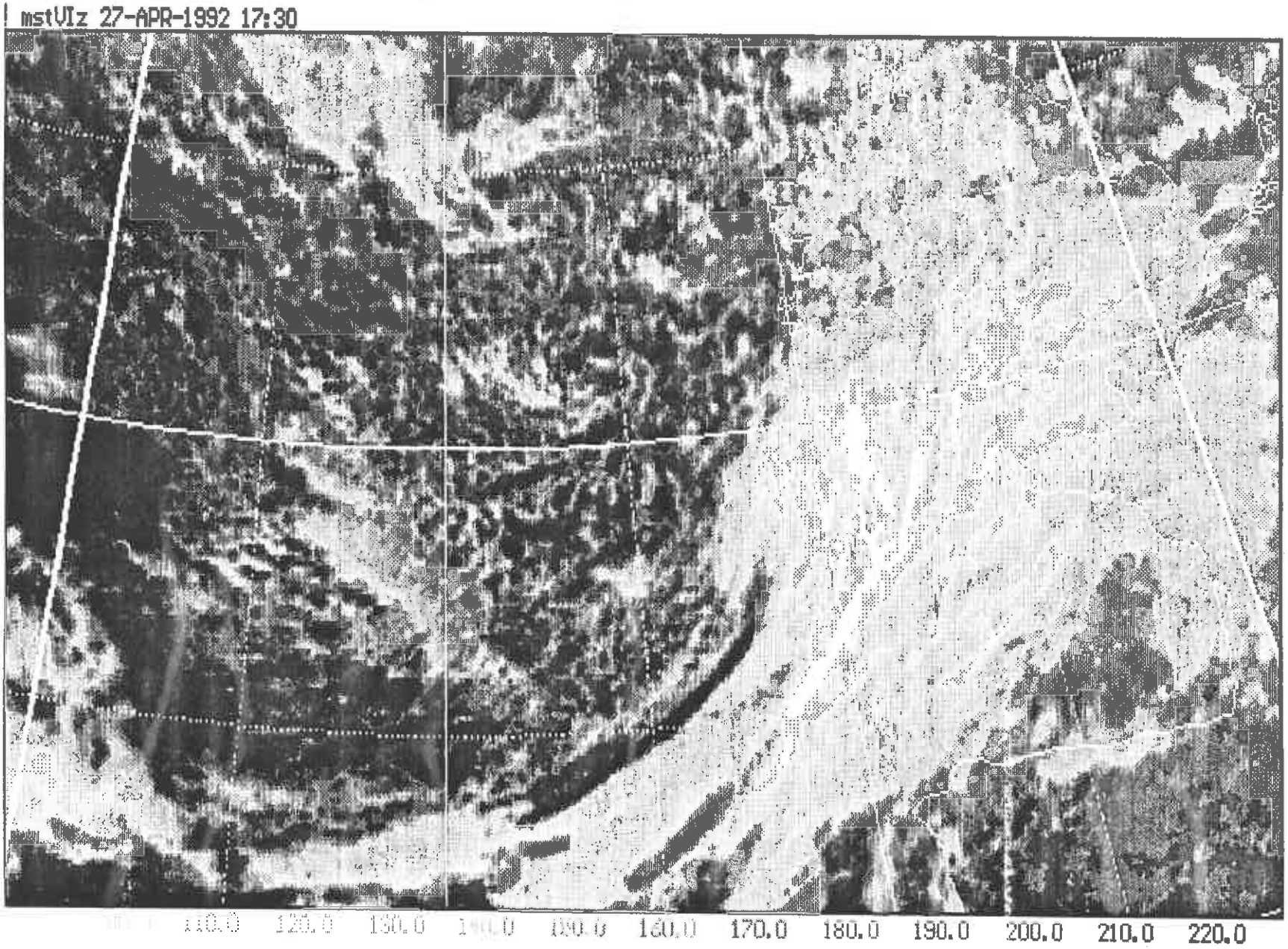

Fig 7

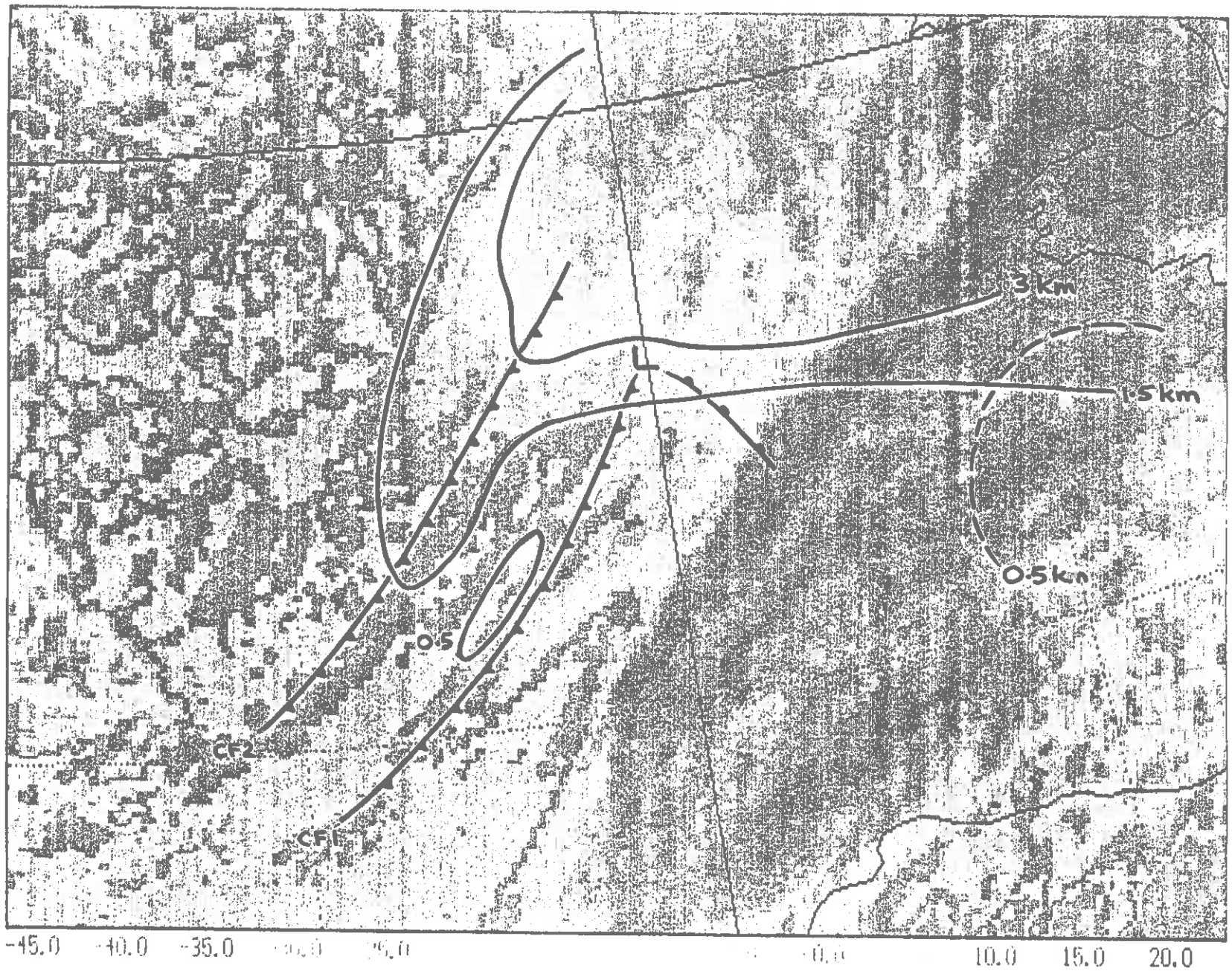

Fig 8

ORIGINAL IN COLOUR

(a)

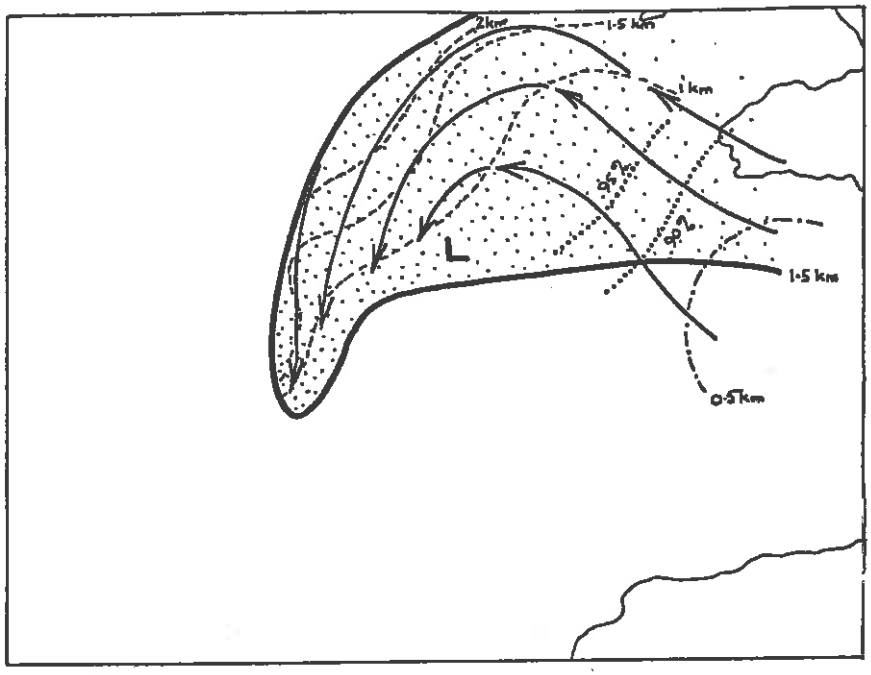
2km
1·5 km
1 km
95%
90%
L
1·5 km
0·5km

(b)

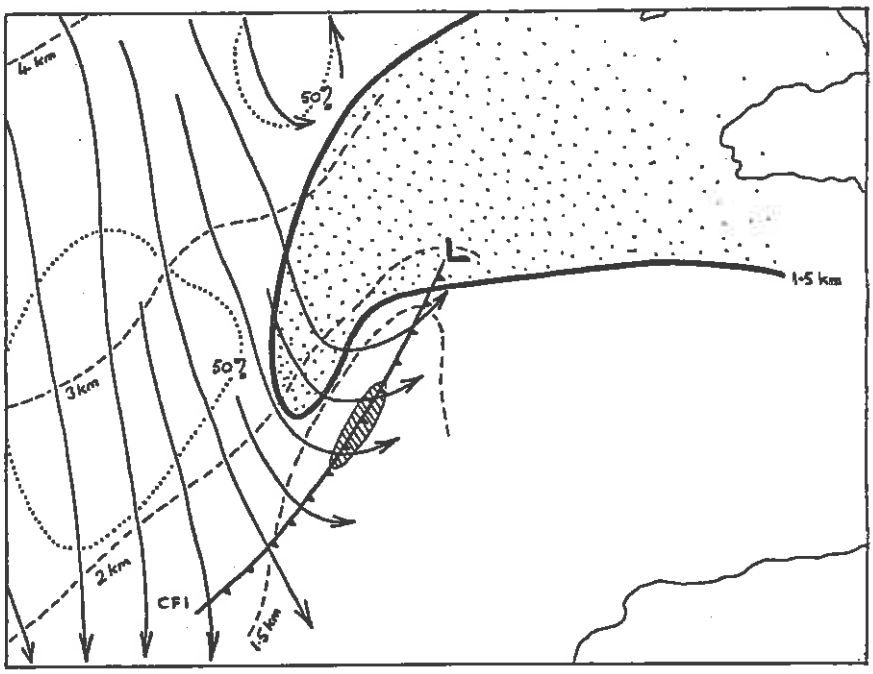
4 km
50%
L
1·5 km
3km
50%
2 km
CF1
1·5km

(c)

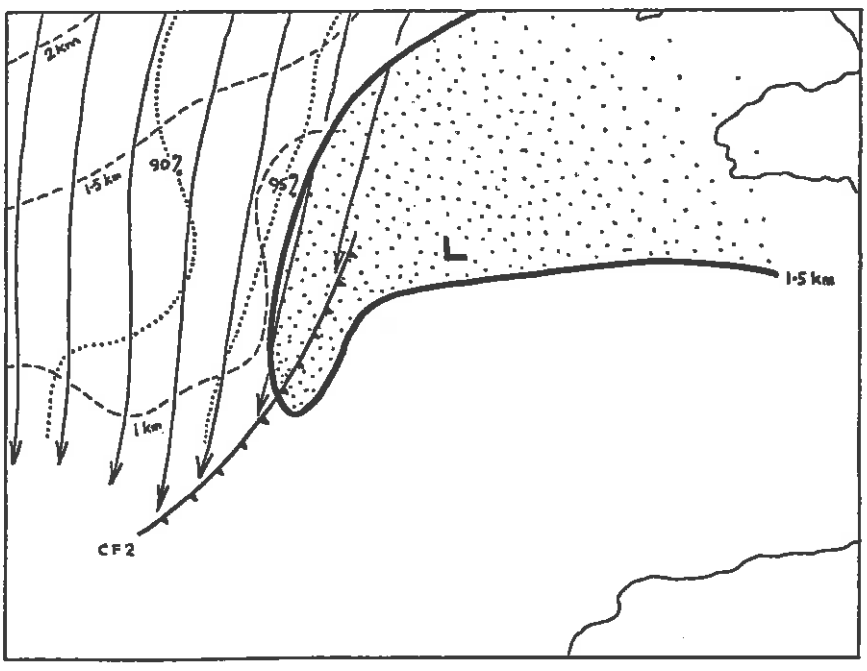
2km
1·5 km
90%
95%
L
1·5 km
1 km
CF2

Fig. 9

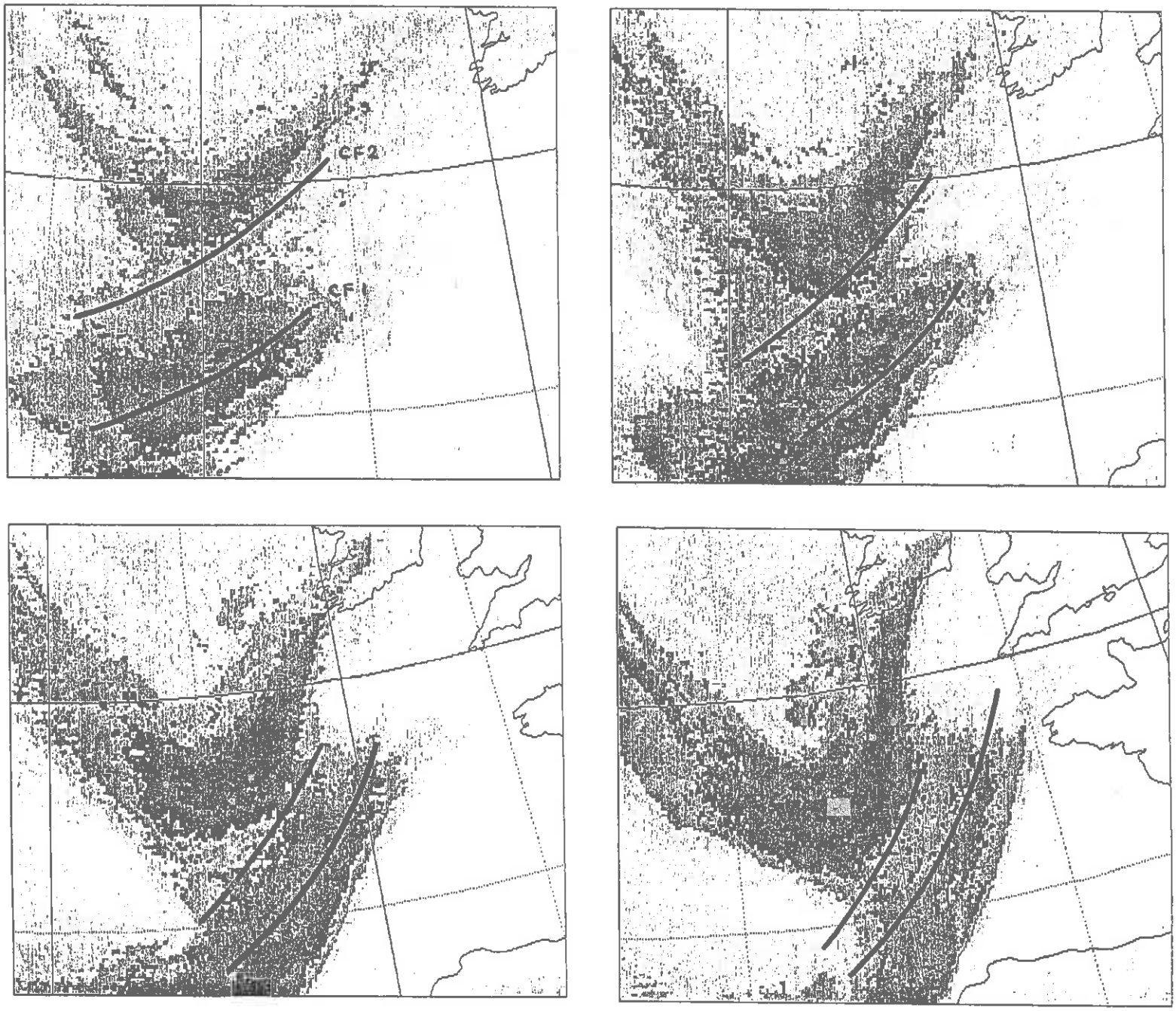

Fig 10

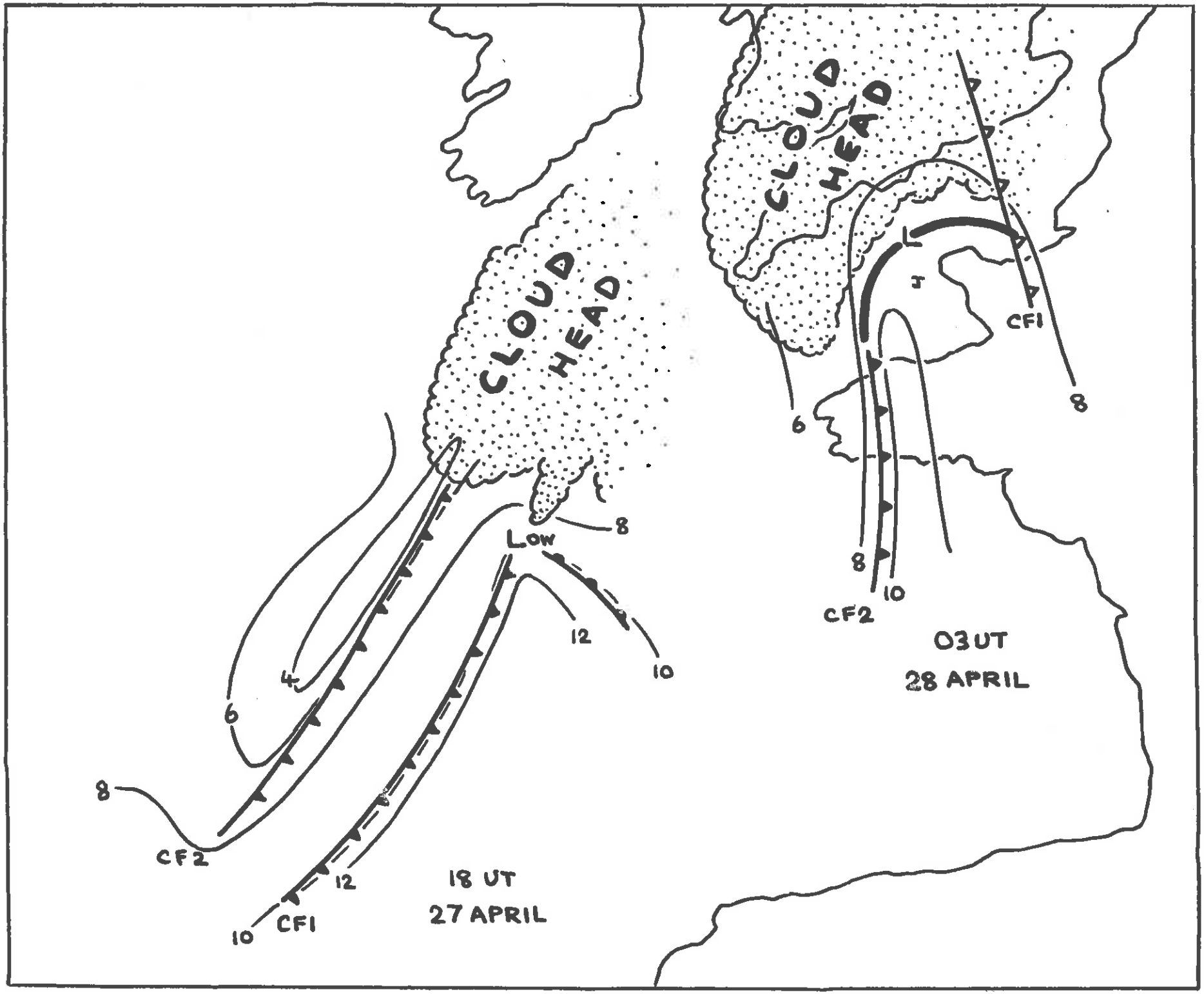
CLOUD HEAD
CLOUD HEAD
Low
8
12
10
4
6
8
CF2
12
10
CF1
18 UT
27 APRIL
L
CF1
6
8
8
10
CF2
03 UT
28 APRIL

Fig 11

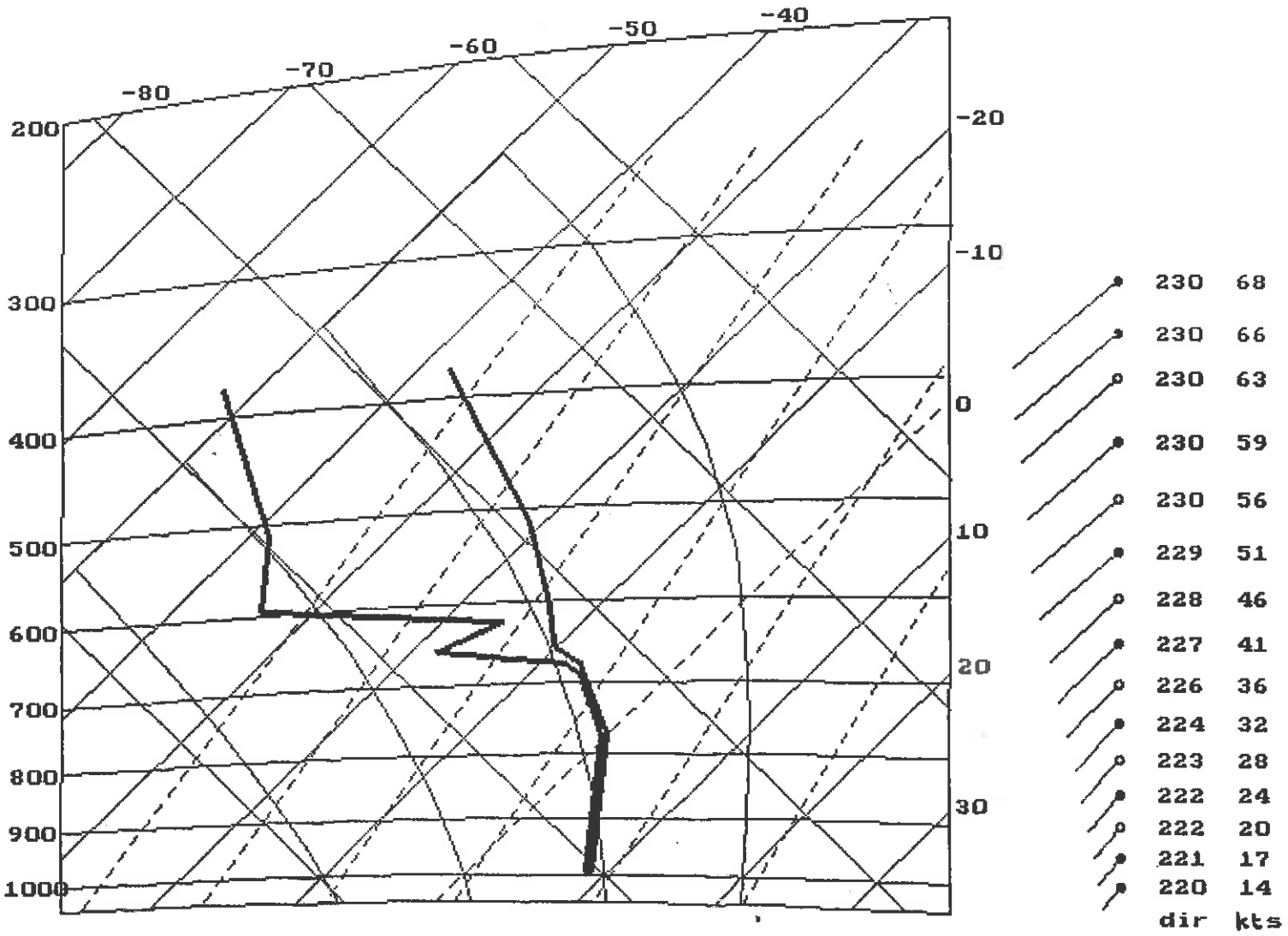
-80
-70
-60
-50
-40
200
300
400
500
600
700
800
900
1000
-20
-10
0
10
20
30
230 68
230 66
230 63
230 59
230 56
229 51
228 46
227 41
226 36
224 32
223 28
222 24
222 20
221 17
220 14
dir kts

Fig 12

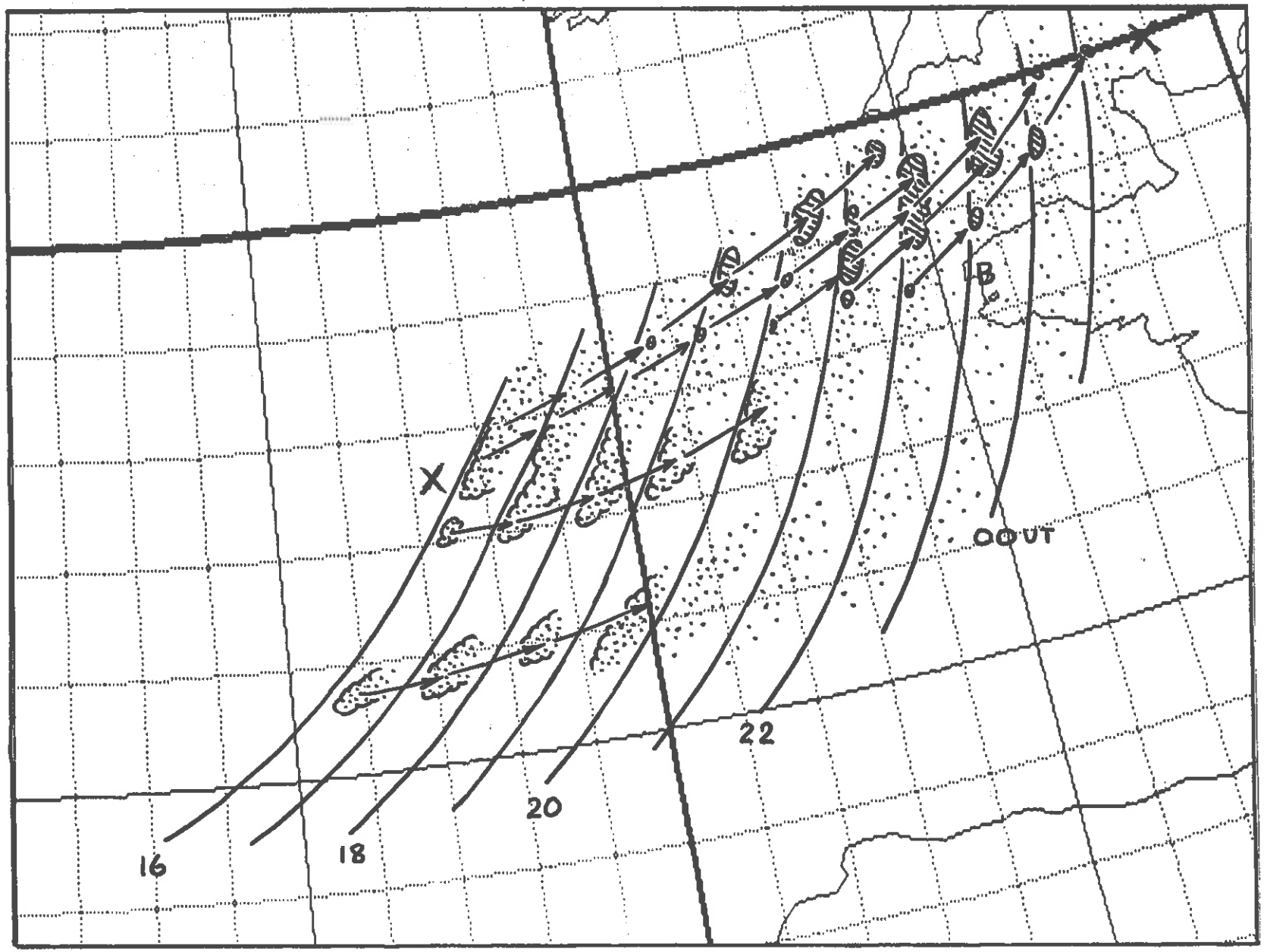

Fig 13

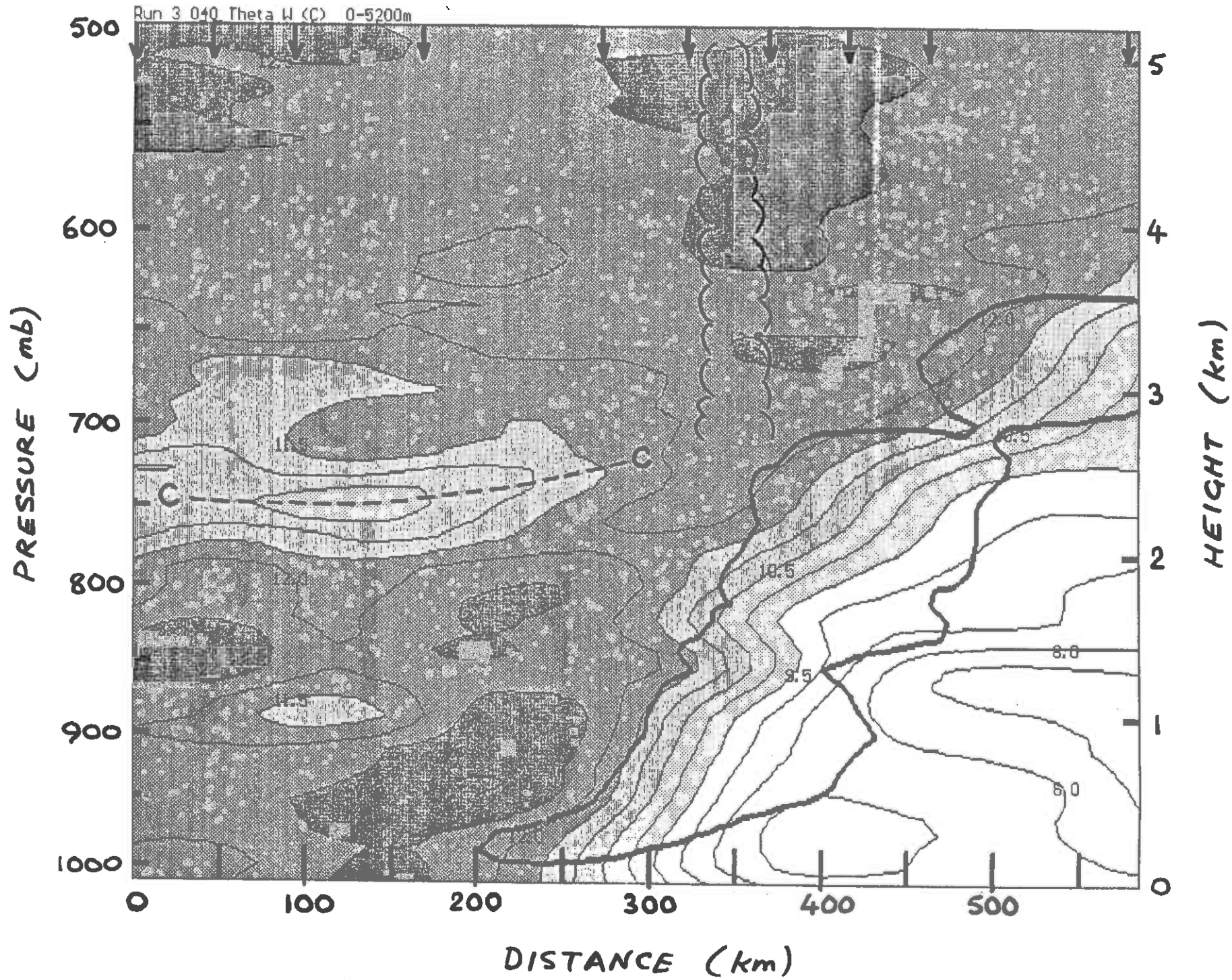
Run 3 040 Theta W (C) 0-5200m
500
600
700
800
900
1000
PRESSURE (mb)
0
100
200
300
400
500
DISTANCE (km)
5
4
3
2
1
0
HEIGHT (km)
C
C
12.0
11.5
10.5
9.5
8.0
6.0

Fig. 14

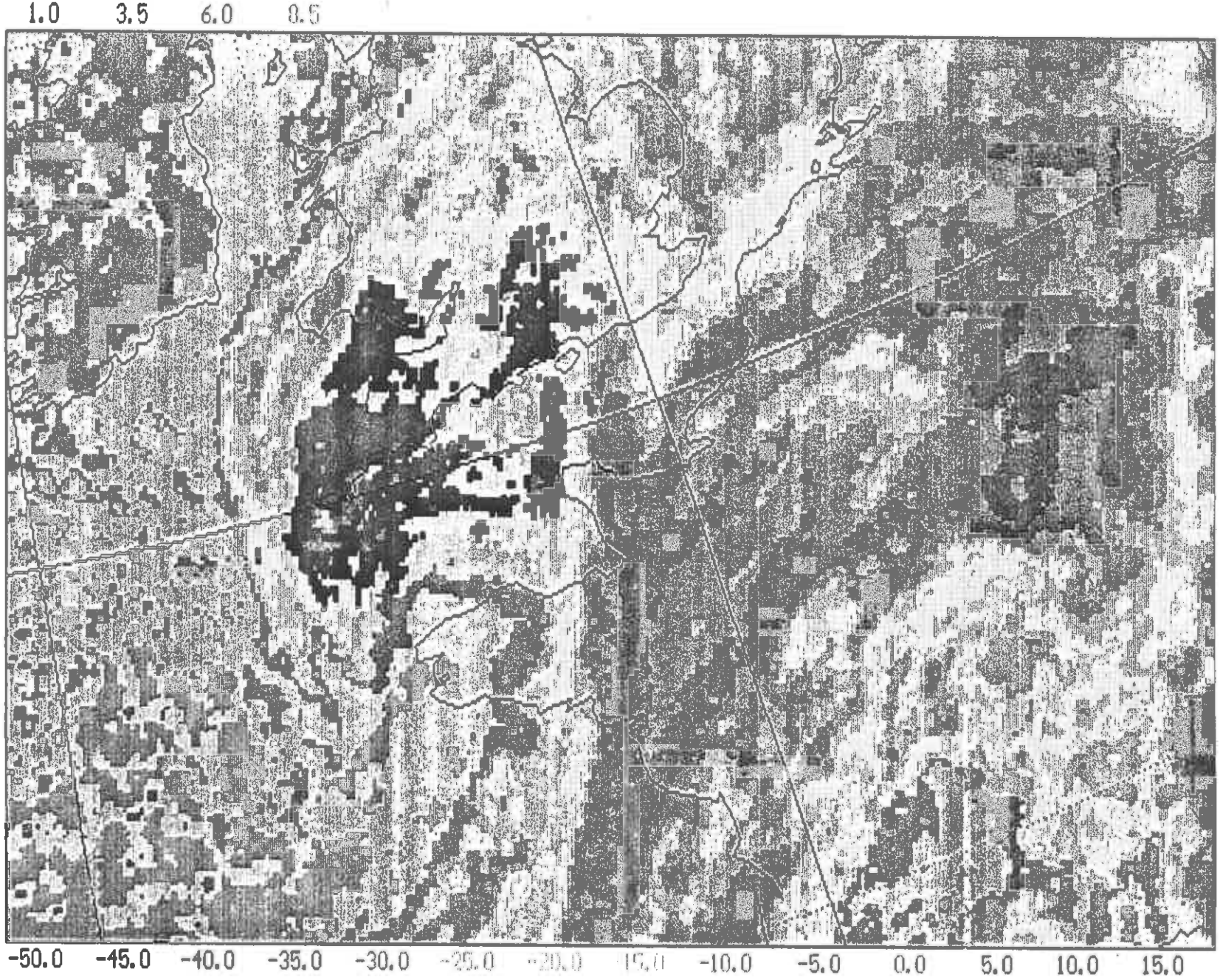

Fig 15

ORIGINAL IN COLOUR

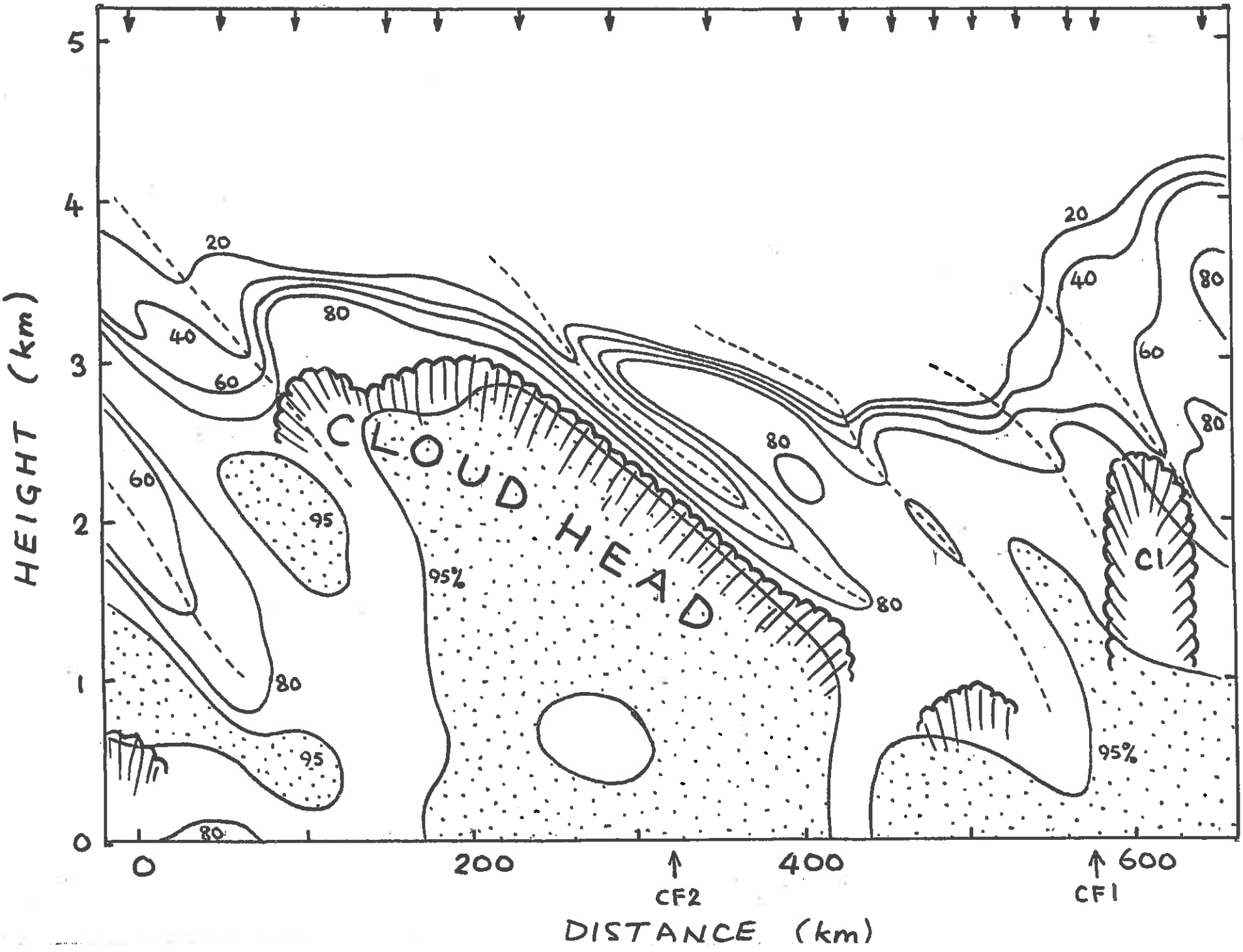
HEIGHT (km)
5
4
3
2
1
0
20
40
60
80
95
95%
CLOUD HEAD
C1
0
200
400
600
CF2
CF1
DISTANCE (km)

Fig 16

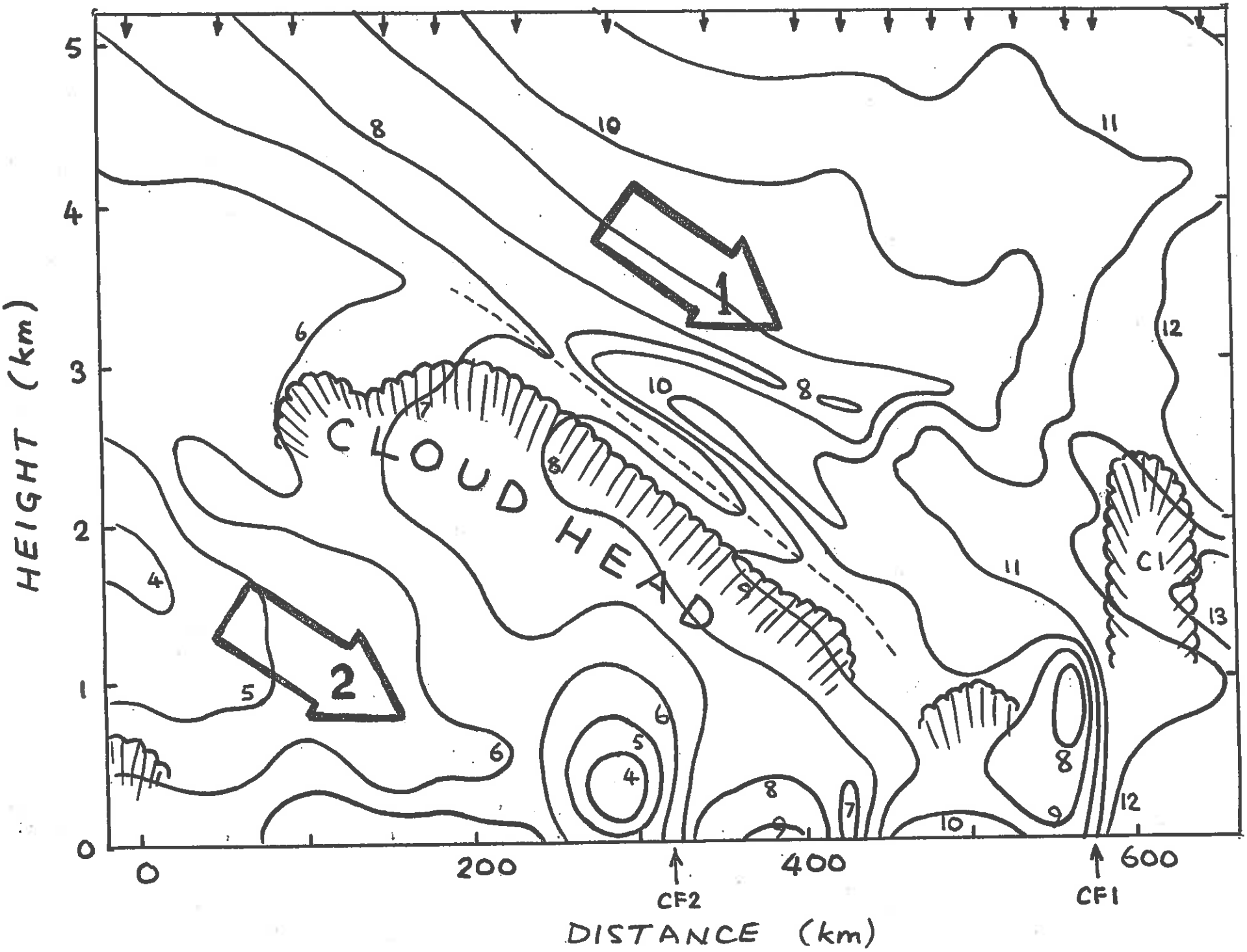
HEIGHT (km)
DISTANCE (km)
CLOUD HEAD
1
2
C1
CF2
CF1
0
200
400
600
0
1
2
3
4
5
6
8
10
11
12
13
7
9

Fig 17

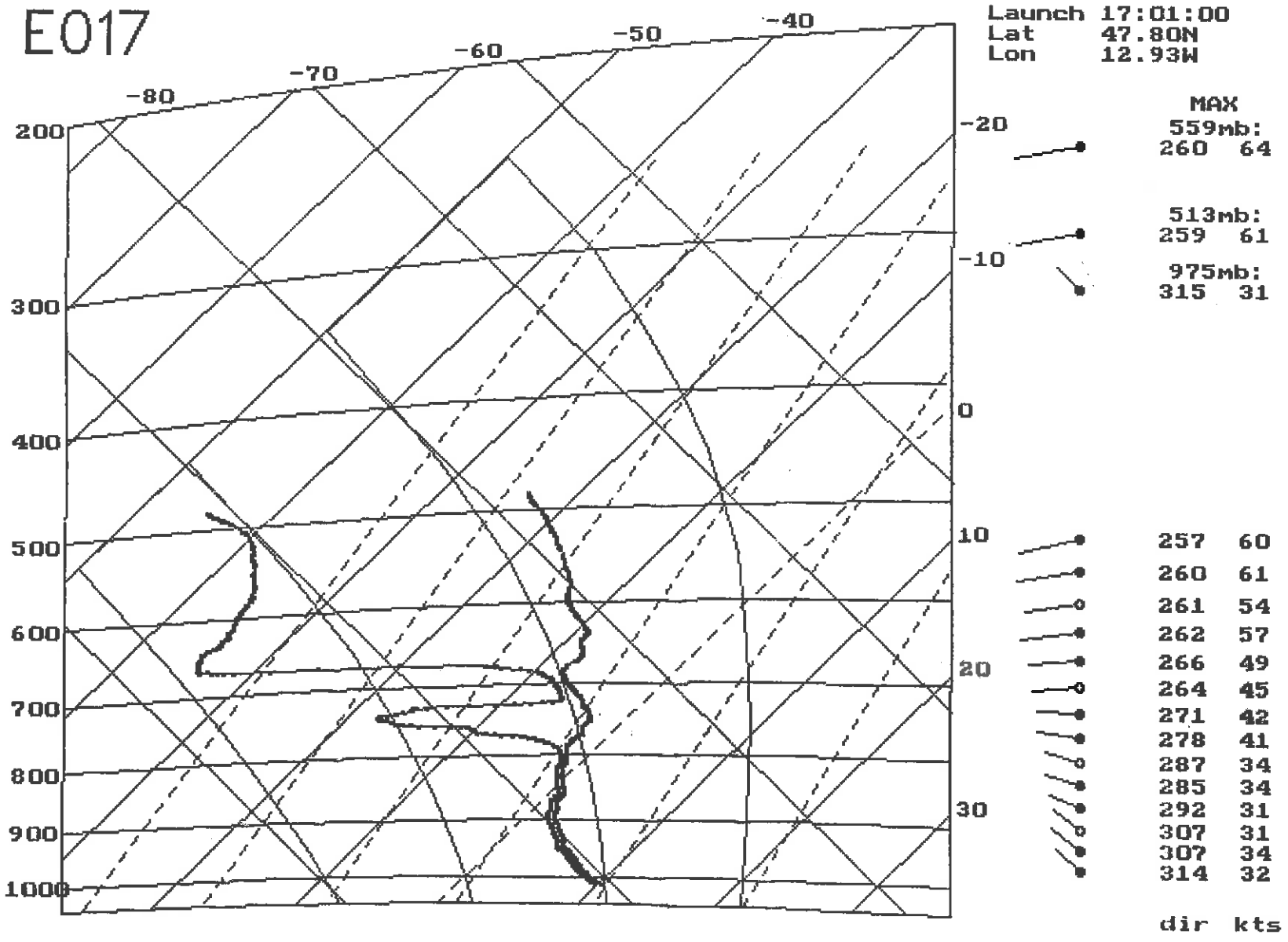
E017
-80
-70
-60
-50
-40
200
300
400
500
600
700
800
900
1000
-20
-10
0
10
20
30
Launch 17:01:00
Lat 47.80N
Lon 12.93W
MAX
559mb:
260 64
513mb:
259 61
975mb:
315 31
257 60
260 61
261 54
262 57
266 49
264 45
271 42
278 41
287 34
285 34
292 31
307 31
307 34
314 32
dir kts

Fig 18(b)

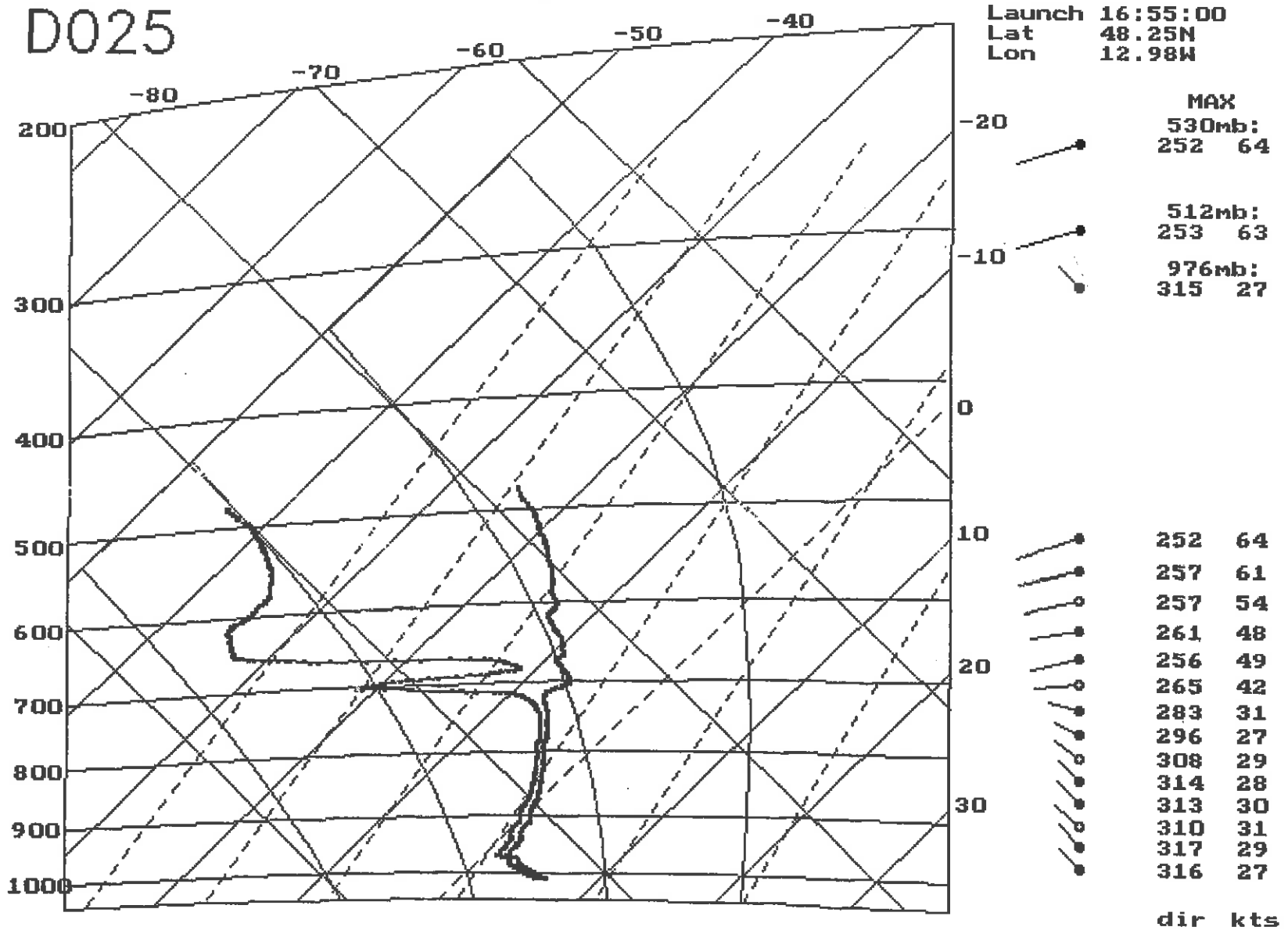
D025
-80
-70
-60
-50
-40
200
300
400
500
600
700
800
900
1000
-20
-10
0
10
20
30
Launch 16:55:00
Lat 48.25N
Lon 12.98W
MAX
530mb:
252 64
512mb:
253 63
976mb:
315 27
252 64
257 61
257 54
261 48
256 49
265 42
283 31
296 27
308 29
314 28
313 30
310 31
317 29
316 27
dir kts

Fig 18(a)

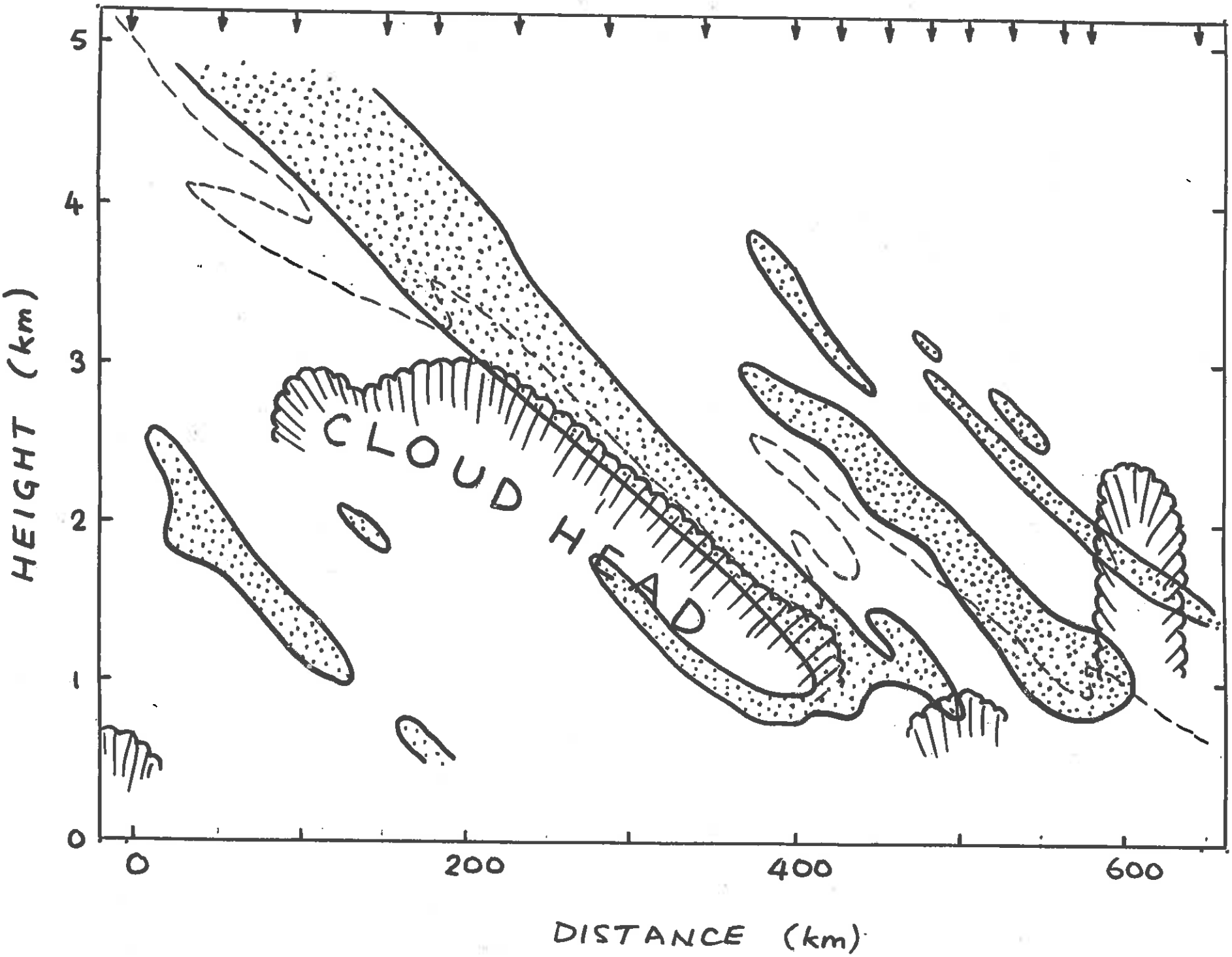

Fig 19

Fig 20(a)

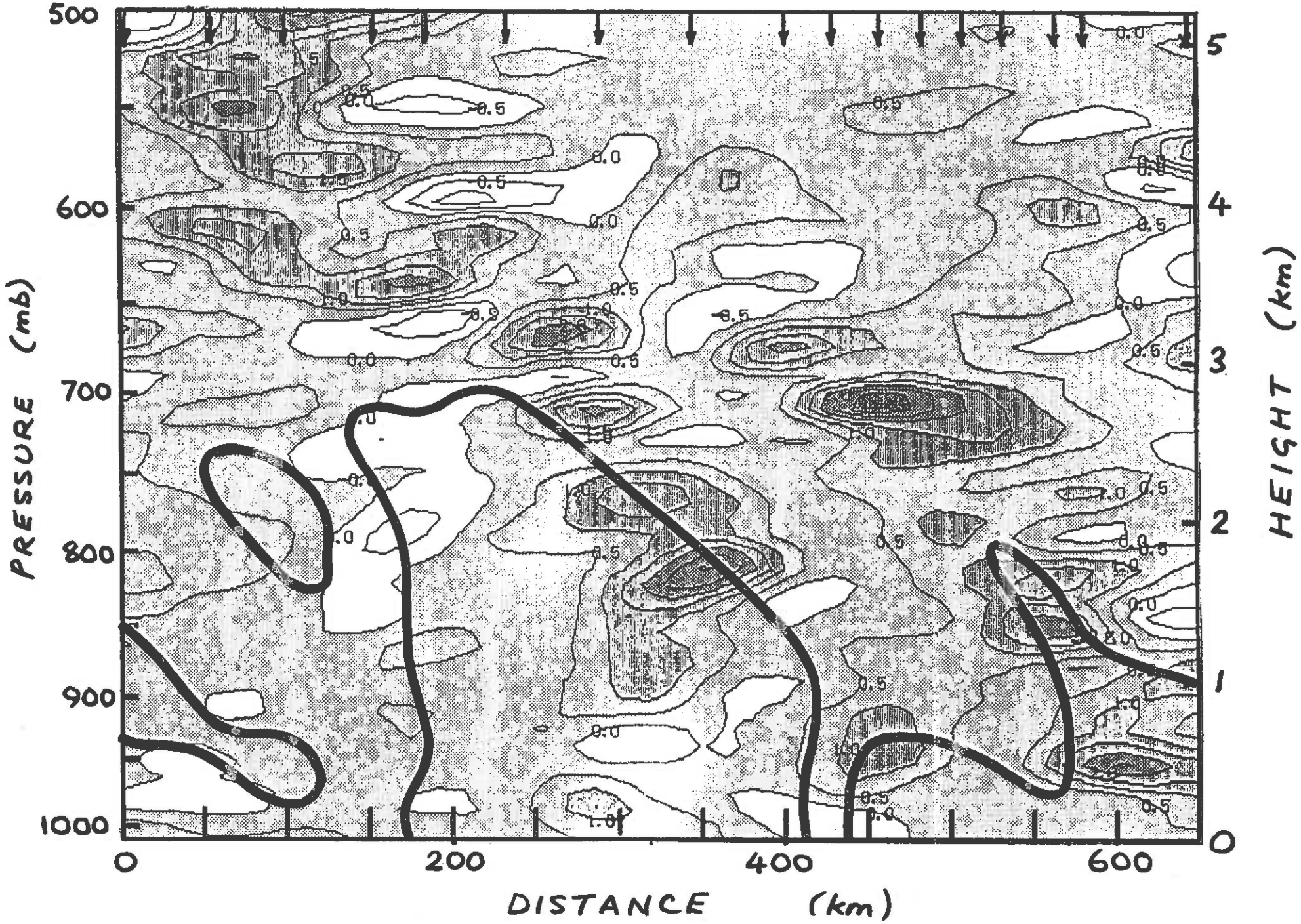
500
600
700
800
900
1000
PRESSURE (mb)
0
200
400
600
DISTANCE (km)
5
4
3
2
1
0
HEIGHT (km)

Fig 20(b)

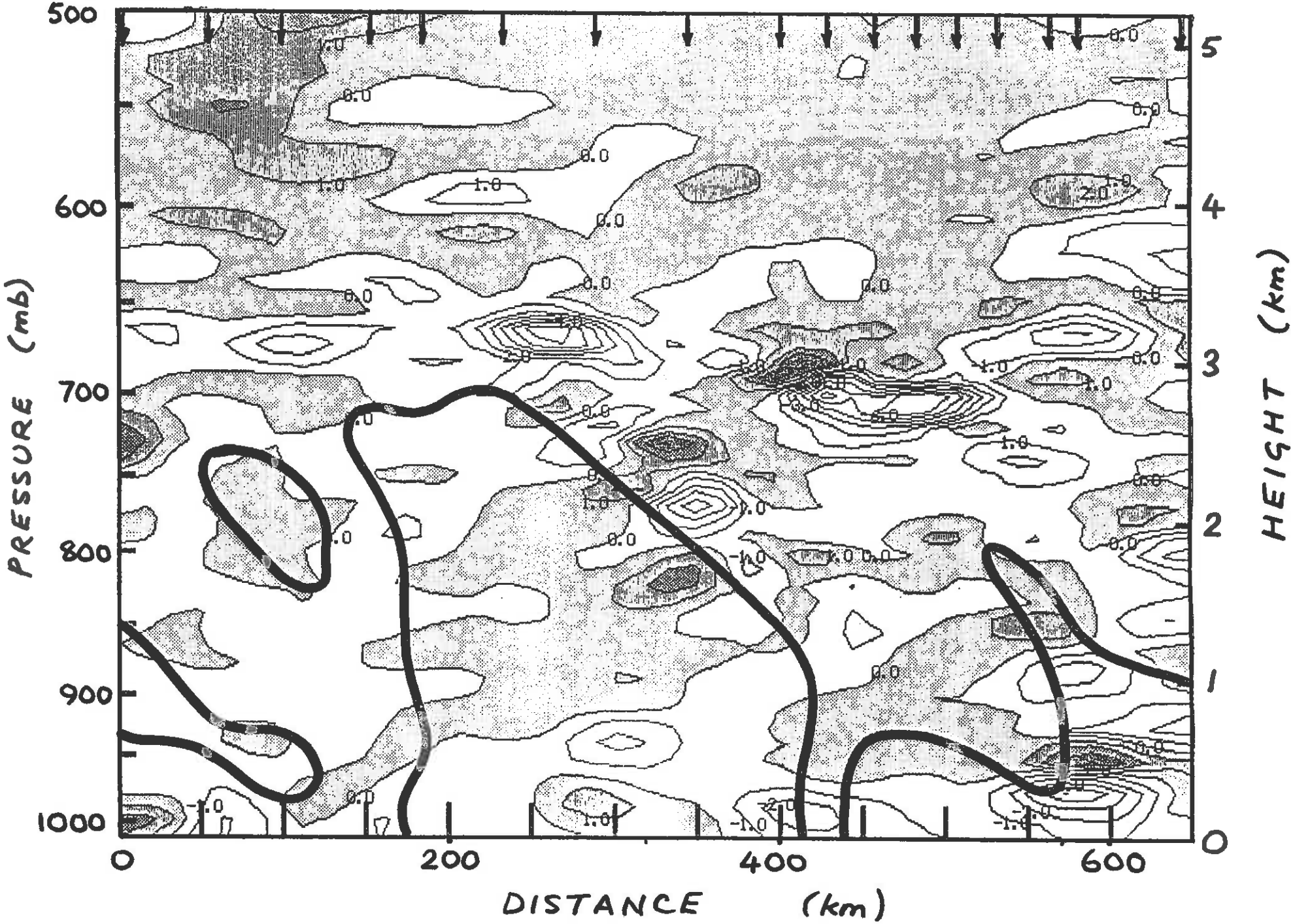
500
600
700
800
900
1000
PRESSURE (mb)
0
200
400
600
DISTANCE (km)
5
4
3
2
1
0
HEIGHT (km)

CURRENT JCMM INTERNAL REPORTS

This series of JCMM Internal Reports, initiated in 1993, contains unpublished reports and also versions of articles submitted for publication. The complete set of Internal Reports is available from the National Meteorological Library on loan, if required.

1. **Research strategy and programme**
   K A Browning et al
   January 1993

2. **The GEWEX Cloud System Study (GCSS)**
   GEWEX Cloud System Science Team
   January 1993

3. **Evolution of a mesoscale upper tropospheric vorticity maximum and comma cloud from a cloud-free two dimensional potential vorticity anomaly**
   K A Browning
   January 1993

4. **The global energy and water cycle**
   K A Browning
   July 1993

5. **Structure of a midlatitude cyclone before occlusion**
   K A Browning and N Roberts
   July 1993

6. **Developments in systems and tools for weather forecasting**
   K A Browning and G Szejwach
   July 1993

7. **Diagnostic study of a narrow cold frontal rainband and severe winds associated with a stratospheric intrusion**
   K A Browning and R Reynolds
   August 1993

8. **Survey of perceived priority issues in the parametrizations of cloud-related processes in GCMs**
   K A Browning
   September 1993

9. **The effect of rain on longwave radiation**
   I Dharssi
   September 1993

10. **Cloud microphysical processes - a description of the parametrization used in the large eddy model**
    H Swann
    October 1993

11. **An appreciation of the meteorological research of Ernst Kleinschmidt**
    A J Thorpe
    May 1992

12. **Potential vorticity of flow along the Alps**
    A J Thorpe, H Volkert and Dietrich Heimann
    August 1992

13. **The representation of fronts**
    A J Thorpe
    January 1993

14. **A parametrization scheme for symmetric instability: test for an idealised flow**
C S Chan and A J Thorpe
February 1993

15. **The Fronts 92 Experiment: a Quicklook Atlas**
Edited by T D Hewson
November 1993

16. **Frontal wave stability during moist deformation frontogenesis**
Part 1: Linear wave dynamics
C H Bishop and A J Thorpe
May 1993

17. **Frontal wave stability during moist deformation frontogenesis**
Part 2. The suppression of non-linear wave development
C H Bishop and A J Thorpe
May 1993

18. **Gravity waves in sheared ducts**
S Monserrat and A J Thorpe
October 1993

19. **Potential vorticity and the electrostatics analogy: quasi-geostrophic theory**
C Bishop and A J Thorpe
November 1993

20. **Recent advances in the measurement of precipitation by radar**
A J Illingworth
April 1993

21. **Micro-physique et givrage: cloud microphysics and aircraft icing**
A J Illingworth
May 1993

22. **Differential phase measurements of precipitation**
M Blackman and A J Illingworth
May 1993

23. **Estimation of effective radius of cloud particles from the radar reflectivity**
N I Fox and A J Illingworth
May 1993

24. **A simple method of Dopplerising a pulsed magnetron radar**
A Hua, A J Illingworth and J Eastment
November 1993

25. **Radiation and polar lows**
George C Craig
February 1994

26. **Collected preprints submitted to the International Symposium on the Life Cycles of Extratropical Cyclones; Bergen, Norway, 27 June - 1 July 1994**
April 1994

27. **Convective frontogenesis**
Douglas J Parker and Alan J Thorpe
April 1994

28. **Improved measurement of the ice water content in cirrus using a total water evaporator**
Philip R A Brown and Peter N Francis
April 1994

29. **Mesoscale effects of a dry intrusion within a vigorous cyclone**
K A Browning and B W Golding
April 1994

30. **GEWEX Cloud System Study, Science Plan**
May 1994

31. **Parametrization of momentum transport by convectively generated gravity waves**
R Kershaw
May 1994

32. **Mesoscale Modelling Newsletter No 5**
May 1994

33. **Observations of the mesoscale sub-structure in the cold air of a developing frontal cyclone**
K A Browning, S A Clough, C S A Davitt, N M Roberts and T D Hewson
May 1994

Met Office Joint Centre for Mesoscale Meteorology Department of Meteorology
University of Reading PO Box 243 Reading RG6 6BB United Kingdom
Tel: +44 (0)118 931 8425 Fax: +44 (0)118 931 8791
www.metoffice.com